Hydrology and
Earth System
Sciences

Multi-decadal floodplain classification and trend analysis in the Upper Columbia River valley, British Columbia

Italo Sampaio Rodrigues[1], **Christopher Hopkinson**[1], **Laura Chasmer**[1], **Ryan J. MacDonald**[1], **Suzanne E. Bayley**[2], and **Brian Brisco**[3],✝

[1]Department of Geography and Environment, University of Lethbridge, Lethbridge, Canada
[2]Department of Biological Sciences, University of Alberta, Edmonton, Canada
[3]Canada Centre for Mapping and Earth Observation, Ottawa, Canada
✝deceased

Correspondence: Italo Sampaio Rodrigues (italo.rodrigues@uleth.ca)

Abstract. Floodplain wetland ecosystems experience significant seasonal water fluctuation over the year, resulting in a dynamic hydroperiod, with a range of vegetation community responses. This paper assesses trends and changes in land cover and hydroclimatological variables, including air temperature, river discharge, and water level in the Upper Columbia River Wetlands (UCRW), British Columbia, Canada. A land cover classification time series from 1984 to 2022 was generated from the Landsat image archive using a random forest algorithm. Peak river flow timing, duration, and anomalies were examined to evaluate temporal coincidence with observed land cover trends. The land cover classifier used to segment changes in wetland area and open water performed well (kappa of 0.82). Over the last 4 decades, observed river discharge and air temperature have increased, precipitation has decreased, the timing of peak flow is earlier, and the flow duration has been reduced. The frequency of both high-discharge events and dry years have increased, indicating a shift towards more extreme floodplain flow behavior. These hydrometeorological changes are associated with a shift in the timing of snowmelt, from April to mid-May, and with seasonal changes in the vegetative communities over the 39-year period. Thus, woody shrubs ($+6\%$ to $+12\%$) have expanded as they gradually replaced marsh and wet-meadow land covers with a reduction in open-water area. This suggests that increasing temperatures have already impacted the regional hydrology, wetland hydroperiod, and floodplain land cover in the Upper Columbia River valley. Overall, there is substantial variation in seasonal and annual land cover, reflecting the dynamic nature of floodplain wetlands, but the results show that the wetlands are drying out with increasing areas of woody/shrub habitat and loss of aquatic habitat. The results suggest that floodplain wetlands, particularly marsh and open-water habitats, are vulnerable to climatic and hydrological changes that could further reduce their areal extent in the future.

1 Introduction

Many montane wetlands have a short history of establishment, due to the short period since the deglaciation of lower-elevation areas (Cooper et al., 2012), and are minerotrophic, making them highly sensitive to changes in surface and groundwater hydrology (Hathaway et al., 2022; Wang et al., 2016, 2018). Large climatic gradients occur within relatively short distances due to elevational changes, which can amplify the effects of climate (MacDonald et al., 1993; Hopkinson and Young, 1998; Loeffler et al., 2011; McCaffrey and Hopkinson, 2020).

Over the last several decades, climatic changes and the amplifying effects of large elevational gradients on microclimatology in the Canadian Rocky Mountains have resulted in significant changes to short-term (Marshall, 2014) and long-term (Edwards et al., 2008; Jost et al., 2012) hydrology, runoff (Stewart et al., 2004), and water storage (Mote et al., 2005; Whitfield, 2001). These changes impact minerotrophic wetlands, which can be sensitive to variations in hydrology;

for example, since the 1950s, the Montane Cordillera Ecozone has experienced precipitation decreases (20 %–50 %) in the southern regions and increases (30 %–50 %) in the northern regions (DeBeer et al., 2016). Changes in the phase of precipitation have also been observed over the last 60 years by Zhang et al. (2000), Schnorbus et al. (2014), and Vincent et al. (2015). On an annual basis, the authors found that the ratio of seasonal snowfall decreased by ~ 8 % in the south and increased by ~ 12 % in the north. The major changes occurred during spring, with reductions of ~ 20 % for the entire region. Furthermore, snow accumulation and duration have also decreased due to a positive trend in air temperature ($+1$ °C since the 1900s) (Zhang et al., 2000; Valeo et al., 2007; Whitfield, 2014), which is leading to earlier and faster snowmelt and glacier melt during spring, resulting in high and shortened peak flows.

By mid-century, peak flows are predicted to increase with a shift to earlier spring runoff. For example, DeBeer et al. (2021) suggest that the timing of runoff could occur up to 2–4 weeks earlier by 2100. Earlier snowmelt increases the length of the summer period, with associated higher air temperatures and evaporative losses (Foster et al., 2016; Leppi et al., 2012). Greater drying potential and diminished summer and autumn streamflow could have broad impacts on the flora and fauna of minerotrophic montane wetlands (Stewart, 2009).

Montane floodplains and the wetlands that exist within them are governed by pulses or short intervals of water runoff, which contribute to flooding (i.e., flood pulses) (Junk et al., 1989). Flood pulses enhance biological productivity and diversity in these ecosystems (Hughes, 1997) associated with the combined effects of the flood timing, water temperature, nutrient content, turbidity, and hydrological connectivity (Stanford et al., 2005; Lacoul and Freedman, 2006; Bayley and Guimond, 2008). Higher-amplitude events that occur over shorter time periods or earlier in the season can inhibit the growth of some species or may initiate succession (Bayley, 1995). For example, during high-flood events (wet years), Amoros and Bornette (2002) observed that fast-flowing river discharge can carry organic nutrients away and deposit silt in the basins, which, according to Sparks et al. (1990) and Bayley and Guimond (2009), may lead to biodiversity decreases or loss, marsh burial, and a change in the wetland. However, in following years, marshes can grow back, as the tubers remain and can regenerate following flooding (Hernandez and Mitsch, 2006). In contrast, periodic dry periods enhance shrub growth, which can be decimated during wet periods (Takaoka and Swanson, 2008).

It is crucial to ascertain whether (1) there is a longer-term trend in the changes that are occurring in these montane floodplains or (2) there are events of such a magnitude that they cause this environment to move into a new ecosystem state. Recent trajectories in montane floodplain wetland land covers remain a source of uncertainty; this raises questions regarding how floodplain riparian vegetation, perma-

nent open water, and discharge properties have increased or decreased over recent decades. Wetland land cover mapping, management, and change assessments typically employ field observation and data collection (Millar et al., 2018; Ray et al., 2019; Windell and Segelquist, 1986); however, this approach is costly, labor-intensive, and unable to represent past conditions (Chasmer et al., 2020).

In this context, remote sensing (RS) data, especially the Landsat time series, can assist in wetland trend and change analysis by providing at least 4 decades of data (Ju and Masek, 2016; Wulder et al., 2022). The Landsat archive, which is now longer than pulses of seasonal or interannual hydroclimatological anomalies, permits the evaluation of longer-term trends across large and spatially continuous areas, thereby helping us to better understand the patterns, direction, rates, and drivers of change in dynamic montane wetland ecosystems.

The Columbia River floodplain in Canada represents a unique environment to assess wetland ecosystem changes over time associated with climatic and land use changes. Wetlands of the Columbia River basin provide important ecosystem services, including acting as critical habitats for flora and fauna, such as spawning grounds for fish (Cooper et al., 2017); supporting food webs (Díaz et al., 2015); filtering and storing sediment from runoff erosion events (Lottig et al., 2013); and accumulating and releasing carbon (Hrach et al., 2022). A better understanding of the trends and changes in this study region will serve as an important reference for other similar wetlands in the Rocky Mountains.

The primary goal of this study is to quantify the floodplain wetland response to changing hydroclimatic conditions within the Upper Columbia River Wetlands (UCRW) in Canada during the past 39 years (1984–2022). The objectives are to quantify and evaluate the historical trends and changes in (i) areal floodplain land cover (open water, marsh, wet meadow, and riparian shrubs and trees) extents within the UCRW and (ii) the peak flow conditions in the Columbia River over the last 39 years in terms of discharge, water level, maximum inundation extent, timing, and duration using remote sensing and river runoff observations. To achieve this, seasonal land cover classifications from Landsat 5 and 8 were generated using a random forest algorithm, and local hydroclimatic data were examined to help explain the observed land cover trends. This study provides a framework for evaluating the effects of climate change in the UCRW, supporting regional decision-makers as part of strategic planning for the local biota and water resource management for the entire Canadian Columbia River.

2 Methods

2.1 Study area

This study focuses on a $\sim 120\,\mathrm{km}$ stretch of the Upper Columbia River floodplain ($188\,\mathrm{km}^2$) between Donald and Invermere within the Rocky Mountain Trench, British Columbia, Canada (Fig. 1). The region drains an upstream area of $\sim 6660\,\mathrm{km}^2$; has historical averages available for air temperature ($3\,°\mathrm{C}$), precipitation ($800\,\mathrm{mm\,yr^{-1}}$; MacDonald and Chernos, 2020), wind speed ($\sim 1\,\mathrm{m\,s^{-1}}$), and relative humidity ($55\,\%$; Hersbach et al., 2020); and the annual average peak flow is $512\,\mathrm{m^3\,s^{-1}}$ (Carli and Bayley, 2015).

2.2 Remote sensing and hydroclimatic data input

The investigation period was 1984–2022, based on the Landsat 5 (TM) and 8 (OLI) Collection-2, Tier-1, Level-2 reflectance archives available via the Google Earth Engine (GEE). GEE contains the Landsat processing methods to compute at-sensor surface reflectance as well as cloud-free composites. Higher-spatial-resolution information (e.g., Sentinel-2, European Space Agency; airborne lidar, Columbia Wetlands Stewardship Partners and the Provincial Government; UAV lidar and geotagged oblique photos; historical aerial photographs, BC Government, 2022) and the historical land cover classification of Canada (Hermosilla et al., 2022) were used together as a reference dataset. To determine the "best available pixel", cloud-free pixels were selected and the median reflectance product was calculated to generate three composition images for each year: (1) prior to seasonal flooding (April to mid-May) – spring; (2) during the peak discharge period (late-May to end July) – summer; and (3) the late-summer hydroperiod (August to mid-September) – late summer. Air temperature and precipitation data for Golden, BC (1984–2022) (Golden A, 1173209; location: $51°17'57''\,\mathrm{N}$, $116°58'56''\,\mathrm{W}$) (Environment Canada, 2022a), and river discharge and water level at the Nicholson gauge (Columbia River at Nicholson, 08NA002; location: $51°14'36''\,\mathrm{N}$, $116°54'46''\,\mathrm{W}$) (Environment Canada, 2022b) on the Columbia River (1903–2022) were obtained from the Environment Canada online data archives.

2.3 Workflow

The UCRW trend and change analysis workflow adopted seven steps, as shown in Fig. 2: (i) acquisition of remote sensing data, (ii) acquisition of hydroclimatic data, (iii) acquisition of reference dataset for classification training purposes, (iv) land cover classification, (v) validation of land covers, (vi) trend analysis, and (vii) land cover change assessment.

2.4 Random forest algorithm and training data collection

To determine changes in the vegetation extent and water extent over time, a random forest (RF) classification (Breiman, 2001) was performed using GEE. RF is a supervised machine learning algorithm that generates multiple decision trees to create and predict a raster classification, in this case four classes: (1) open water, (2) marsh (i.e., bulrush, *Schoenoplectus tabernaemontani*, and cattail marsh, *Typha latifolia*), (3) wet meadow (e.g., beaked sedge, *Carex rostrata*; water sedge, *Carex aquatilis*; and horsetail, *Equisetum arvense*), and (4) woody/shrub vegetation (e.g., woody species include cottonwood, *Populus*; Norway spruce, *Picea abies*; and dogwood, *Cornus* spp.; and shrub species include Sitka willow, *Salix sitchensis*; red osier dogwood, *Cornus sericea*; and horsetail, *Equisetum* spp.). RF was used because it is non-parametric and does not rely on a priori knowledge of the ecological drivers or characteristics of the prediction/classification outputs (Menze et al., 2009).

Training data collection, however, can be challenging over large or mountainous regions, as these ecosystems have dynamic or unpredictable weather and are remote and difficult to enter (e.g., Inglada et al., 2017). Moreover, access to training data is difficult to acquire over time because data may not be available for the period of assessment; land cover classes or observations could also be different from the current study, making comparison difficult. In this research, we utilize a variety of reference remote sensing data sources – UAV and airborne lidar, aerial photographs, geotagged photos, Sentinel-2, and historical classified land cover (Hermosilla et al., 2022) – to generate training samples per each year (Fig. 1).

To extract or determine the most reliable training pixels within areas of unchanging land cover class, the time series classification of Hermosilla et al. (2022) was used. Land cover permanence was calculated by summing the number of times each land cover class pixel was identified in the same pixel location. Reference rasters contain a numerical pixel value (i.e., 1 – open water; 2 – marsh; 3 – wet meadow; 4 – woody/shrub) that corresponds to each land cover in the input rasters. The 1984 land cover raster was chosen as the reference raster because this was the first year of the record, thereby providing a baseline or starting point from which to compare. The permanent land cover raster was then used within GEE to mask out permanent zones within the study floodplain that showed potential as training areas. Training pixels were subsequently allocated within these training areas and used over the whole time series. However, in the years with available higher-resolution imagery (i.e., sporadically throughout the time series: aerial photographs – 1984 to 1991, 2005, 2007, and 2009; Sentinel-2 – 2016 to 2022; airborne lidar – 2018; UAV lidar and geotagged photos – 2022), it was possible, by expert interpretive identification of land cover class, to increase the number of training pixels with more reference datasets.
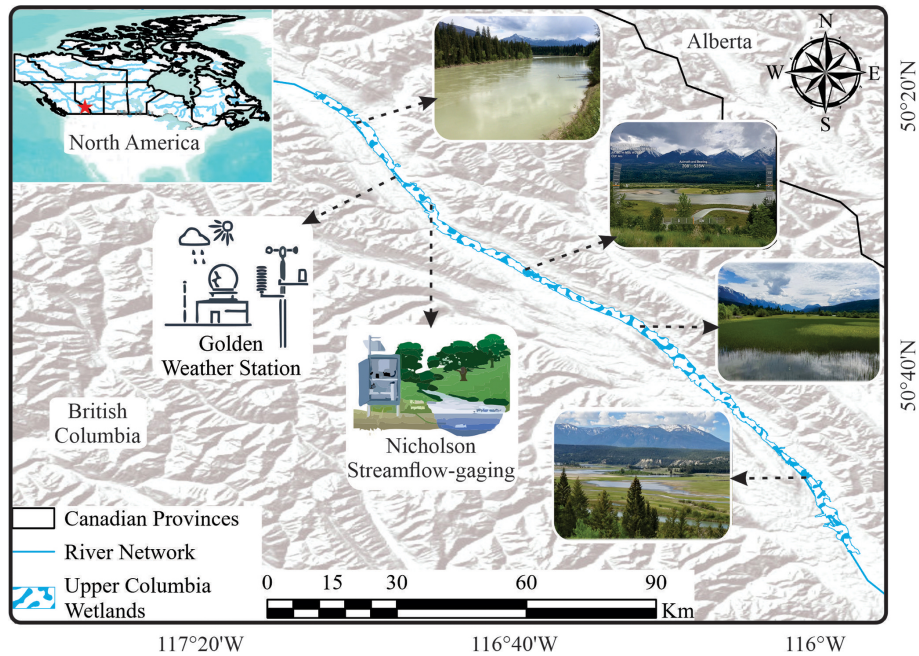
Figure 1. Study area and approximate location of the streamflow gaging and weather station.
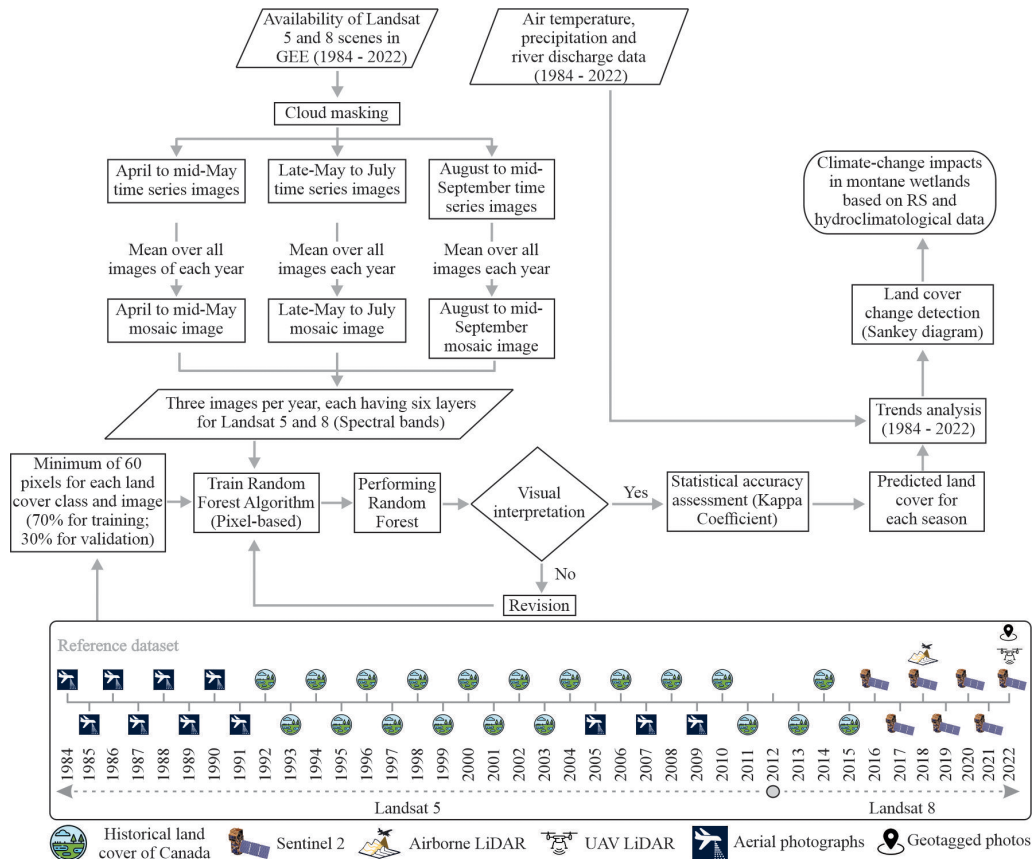

Figure 2. Methodological workflow for the spatial–temporal (1984–2022) analysis of vegetated and water land cover classes using remote sensing and hydroclimatological data.

To reduce the uncertainty in the training data associated with classification errors in the historical land cover classification (Hermosilla et al., 2022), pixels within land cover patches were selected. Therefore, training pixels had to be at least 90m from adjacent land covers (to reduce the potential for edge effects and mixed pixels) (Pelletier et al., 2016). The RF model was trained using 1500 trees (as per Millard and Richardson, 2015), and each class sample had a minimum of 60 pixels identified (60 pixels per land cover class; a total of 240 for the four land cover classes), and in the years with available higher-resolution imagery, > 40 pixels per land cover class were allocated (about 100 pixels per land cover class; a total of 400 assuming the four land cover classes), with 70 % used for training and 30 % reserved for validation. Pixels reserved for training within the RF model were those that were furthest in distance from clouds or cloud shadow boundaries, as applied in White et al. (2014). The training pixels were randomly distributed across the study floodplain with each scene mosaic. Classification was performed using the five following Landsat TM and OLI bands: blue (Band 2 in OLI; Band 1 in TM), green (Band 3 in OLI; Band 2 in TM), red (Band 4 in OLI; Band 3 in TM), near-infrared (NIR, Band 5 in OLI; Bands 4 and 5 in TM), and shortwave infrared (SWIR, Bands 6 and 7 in OLI; Band 7 in TM). Figure 3 illustrates the training and validation steps and the location of the training sites.

2.5 Reference dataset and accuracy measurement

The higher-spatial-resolution RS, such as UAV and airborne lidar, aerial photographs, Sentinel-2, geotagged photos, and the unchanging pixels of the Historical Land Cover of Canada created by Hermosilla et al. (2022), were used to allocate the training pixels/polygons (for more details, see the Supplement). Thereafter, the kappa coefficient was calculated to estimate the accuracy of the RF-simulated land cover.

According to Congalton and Green (2019), 50 random ground sample points are enough for each land cover category, although a minimum of 200 samples were used per mosaic image. The results of the kappa accuracy assessment were then summarized in a confusion matrix with omissions and commissions for all classes and periods. Furthermore, as discharge and open-water area are expected to covary, a linear regression between these two variables was performed: (i) as an additional check on the open-water classification and (ii) to create a discharge-based model of floodplain inundation area.

2.6 Trend and change analysis

To assess the trends over 39 years in the wetland area classification and the hydroclimatic data, a Mann–Kendall (Mann, 1945; Kendall, 1975) test was performed using pyMannKendall (Hussain and Mahmud, 2019). The Mann–Kendall method is a nonparametric test used to identify a trend in a series. To evaluate changes in wetland extent, three hypotheses were tested based on trends over the period of data observation: (i) no trend exists over the time period, (ii) a positive trend exists, and (iii) a negative trend exists. A significance level or p value ≤ 0.05 was assumed. For the land cover change assessment, the Change Detection Wizard in ArcGIS Pro was used with a pixel value change method to assess the shift during 1984–2022 raster datasets.

## 2.7 Discharge timing, duration, frequency, hydrograph, and anomaly assessment

To understand how hydroclimate variability might have influenced or altered wetland extents throughout the time of study, the use of direct observation (stream gaging) methods is an appropriate way to evaluate river-based wetland changes. The timing and length of the peak flow were determined using the historical streamflow gaging station from Nicholson (1903–2022). The data were divided using a 25-year time interval to assess when the peak flow occurred and how it has changed since 1903 (compared groups: 1903–1928, 1929–1953, 1954–1978, 1979–2003, and 2004–2022). This time interval was chosen because the Pacific Decadal Oscillation (PDO) influences precipitation and air temperature in the central eastern Rocky Mountains (Linsley et al., 2015), and the PDO periodicities/cycles were most energetic/perceptive within a 25-year interval average (Mantua and Hare, 2002). To determine whether the peak flow is occurring earlier or later, an average of the Julian day peak flow for each group was calculated and then compared.

The 10 % highest daily river flow/discharge (relative to the river peak flow/discharge) for each year was determined for the peak flow duration/length as well as the number of days. To ascertain if the number of peak flow days is increasing or decreasing, the data were further divided into the five aforementioned groups. The average of the number of peak flow days per 25-year time interval was determined and then compared.

To define the distribution of river discharge and how it changed over the course of a century, a frequency (%) curve from the daily and peak discharge was built, using the same five groups (1903–1928, 1929–1953, 1954–1978, 1979–2003, and 2004–2022), to show the frequency of each flow discharge as well as the frequency with which it is overcome. Additionally, a peak flow hydrograph analysis was carried out for the five groups using the 25-year period interval average to compare the shape and how it has changed since 1903. To separate the peak flow from baseflow, the recession method (Brutsaert and Nieber, 1977) was used:

$$Q_{\mathrm{t}} = Q_0 K^t, \tag{1}$$

where Q_{t} is the baseflow (the threshold utilized was $50\,\mathrm{m}^3\,\mathrm{s}^{-1}$ because it was observed that the discharge normally only increased beyond this value), Q_0 is the initial
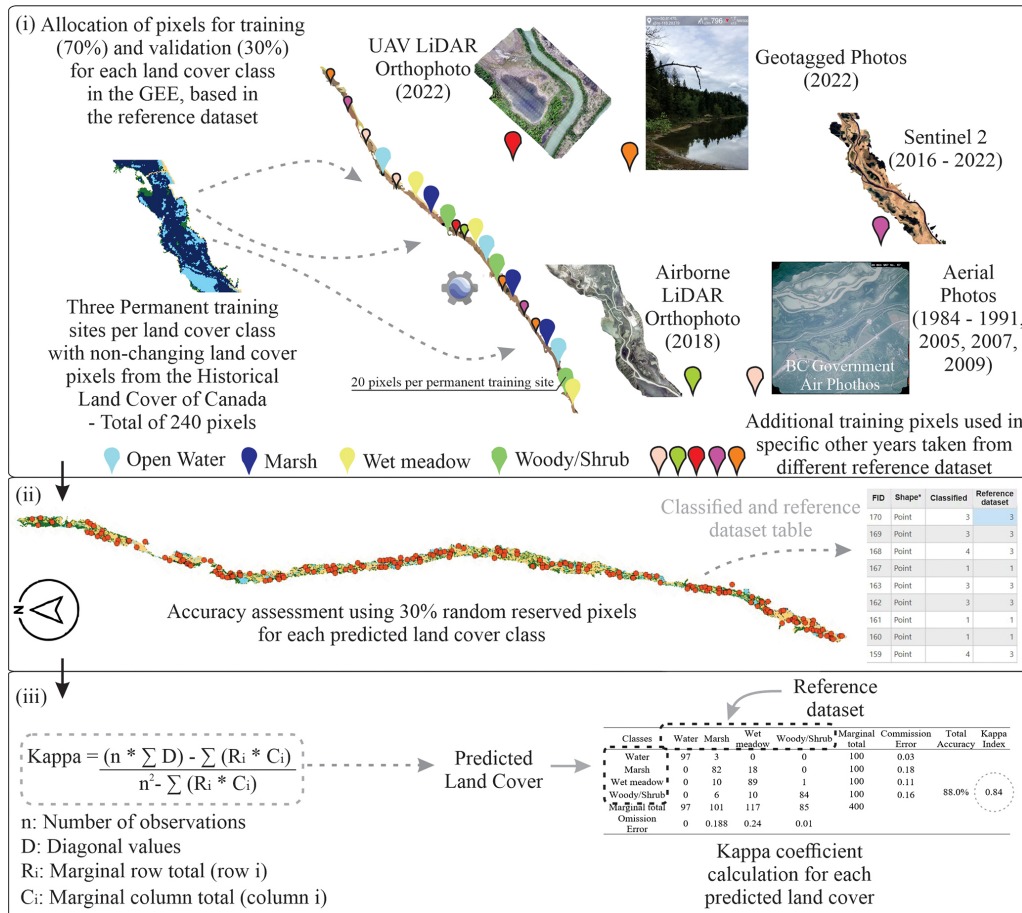
Figure 3. Steps for land cover prediction: **(i)** allocation of training pixel method; **(ii)** accuracy assessment for the predicted land cover; **(iii)** statistical evaluation using the kappa coefficient.

baseflow (at the beginning of the storm event, time $= 0$), k is the exponential decay constant (ratio of the baseflow at time $t = 0$ to the baseflow 1 d earlier), and t is the number of days after the start of the peak flow. This method is used to discover the daily baseflow during the peak flow, and Eq. (2) is used to determine the peak flow runoff (Q_{PR}).

$$Q_{PR} = Q - Q_t \tag{2}$$

After finding Q_{PR}, the values were plotted to create a hydrograph, and an exponential model (Eq. 3) was generated for each hydrograph to determine the recession constant (α), where a larger α represents a steeper decline (Berhail et al., 2012).

$$Q_a = Q_i e^{-\alpha t} \tag{3}$$

Here, Q_a is the discharge at time t after recession, Q_i represents the discharge at the start of recession, and e is Euler's number (2.71828). In terms of the anomaly evaluation, it was used to identify how climate change affected peak discharge. The anomaly assessment was also used to detect the predominant PDO pattern (i.e., warm, normal, or cold) in each 25-year interval in the UCRW. We employed a straightforward

technique suggested by Genz and Luz (2012). The anomaly for the peak flow was determined as follows:

$$anomaly = \frac{(Q_i - Q_m)}{\sigma}, \tag{4}$$

where Q_i is the annual peak flow (m^3 s^{-1}) in a year, Q_m is the historical average of peak flow (m^3 s^{-1}), and σ is the standard deviation (m^3 s^{-1}). The anomaly can be classified as wet > 0.5, normal year ± 0.5, or dry < -0.5. A Mann–Kendall trend test was then used to assess the anomalies to determine whether or not the peak flow anomaly was increasing or decreasing.

3 Results

3.1 Random forest classification accuracy

An RF classification was used to determine the land cover extent per season in the UCRW from 1984 to 2022. To do this, 100 supervised classifications were performed for each period of spring (37), summer (29), and late summer (34), us-
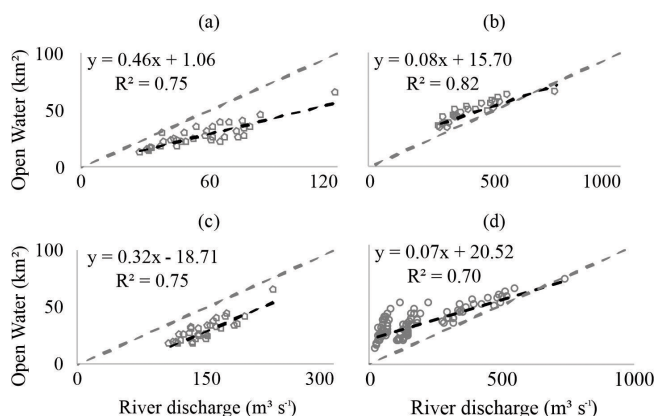
Figure 4. Linear regression between open-water area and river discharge in **(a)** April to mid-May, **(b)** late-May to July, **(c)** August to mid-September, and **(d)** on an annual basis.

ing a total of 32 880 pixels for all seasonal images (23 016 for training and 9864 for validation). The average kappa coefficient for all land cover classes and from each study period was 0.83 (April to mid-May; Supplement Tables S1–S37), 0.85 (late-May to July; Tables S38–S66), and 0.78 (August to mid-September; Tables S67–S100), resulting in an average for all images of 0.82 (all confusion matrices with total accuracy, omission, and commission for all classes and periods as well as their corresponding classified raster are given in Tables S1–S100 in the Supplement). Furthermore, the area of open water was correlated with river discharge for each year (Fig. 4), with R^2 values varying from 0.75 (April to mid-May and August to mid-September) to 0.82 (late-May to July). This is not a direct validation of the open-water classification; however, as river discharge increases, open-water extent across the floodplain also increases.

3.2 Changes in the Upper Columbia floodplain from 1984 to 2022

The area of open water decreased from April to mid-May ($-0.11 \, \text{km}^2 \, \text{yr}^{-1}$, $-5 \, \text{km}^2$ or $-3 \, \%$ in 39 years, compared with the UCRW area) and from August to mid-September ($-0.28 \, \text{km}^2 \, \text{yr}^{-1}$, $-11 \, \text{km}^2$ or $-6 \, \%$), which might be related to an overall reduction in precipitation ($-0.75 \, \text{mm} \, \text{yr}^{-1}$; p value $= 0.01$) and an increase in air temperature ($0.02 \, °\text{C} \, \text{yr}^{-1}$; p value $= 0.02$) since 1984. The decrease in precipitation may have resulted in a loss of marsh areas of $-1.39 \, \text{km}^2 \, \text{yr}^{-1}$ ($-55 \, \text{km}^2$ or $-29 \, \%$) during spring and $-0.24 \, \text{km}^2 \, \text{yr}^{-1}$ ($-9 \, \text{km}^2$ or $-5 \, \%$) by late summer, an increase in wet-meadow area during spring ($1.28 \, \text{km}^2 \, \text{yr}^{-1}$, $+48 \, \text{km}^2$, $+26 \, \%$), and a reduction in wet-meadow area in the late summer ($-0.12 \, \text{km}^2 \, \text{yr}^{-1}$, $-4 \, \text{km}^2$, $-2 \, \%$). In contrast, woody/shrub vegetation increased in area over the spring, peak flow period, and late summer by $0.26 \, \text{km}^2 \, \text{yr}^{-1}$ ($+11 \, \text{km}^2$, $+6 \, \%$), $0.50 \, \text{km}^2 \, \text{yr}^{-1}$ ($+20 \, \text{km}^2$, $+11 \, \%$), and $0.57 \, \text{km}^2 \, \text{yr}^{-1}$ ($22 \, \text{km}^2$, $+12 \, \%$), respectively.

During the peak flow season (late-May to July), the open-water extent showed a positive tendency ($0.13 \, \text{km}^2 \, \text{yr}^{-1}$, $+3 \, \%$), likely due to the increase in peak discharge ($0.58 \, \text{m}^3 \, \text{s}^{-1} \, \text{yr}^{-1}$; p value $= 0.02$) and water level ($0.63 \, \text{cm} \, \text{yr}^{-1}$; p value $= 0.02$), and may be related to the increase in air temperature, which influences the beginning of the snowmelt period. This rapid and earlier rise in open water during the summer may have a negative impact on marsh growth, which may explain the negative trend of $-0.90 \, \text{km}^2 \, \text{yr}^{-1}$ in marsh area in this period ($-19 \, \%$) in the flood basin. The marsh areas declined and were replaced by more open water ($0.13 \, \text{km}^2 \, \text{yr}^{-1}$, $+3 \, \%$), and an increase in the area of wet meadow ($0.30 \, \text{km}^2 \, \text{yr}^{-1}$, $+7 \, \%$) and woody/shrub ($0.50 \, \text{km}^2 \, \text{yr}^{-1}$, $+11 \, \%$) over the 39 years in the summer period.

The trends in the land cover extent and hydroclimatological indicators are shown in Fig. 5 and Table 1, respectively. The overall annual trends show that open-water ($-0.03 \, \text{km}^2 \, \text{yr}^{-1}$) and marsh ($-0.10 \, \text{km}^2 \, \text{yr}^{-1}$) extent are decreasing, whereas wet meadow ($0.06 \, \text{km}^2 \, \text{yr}^{-1}$) and woody/shrub ($0.17 \, \text{km}^2 \, \text{yr}^{-1}$) areas are expanding (Fig. 5d). The relatively small annual changes compared with the larger seasonal changes (Fig. 5d vs. 5a, b, and c) demonstrate the importance of the seasonal evaluation in detecting changes in the UCRW. The spatial context and the percentage change during spring, summer, and late summer in Figs. 6, 7, and 8, respectively, shows how each land cover has changed over 39 years in the floodplain. The location/coordinates of the main changes are provided in the Supplement (Tables S101–S104).

3.3 Upper Columbia River discharge

The average discharge (Q_m) of the Upper Columbia River was $428.2 \, \text{m}^3 \, \text{s}^{-1}$ with a standard deviation (σ) of $105.9 \, \text{m}^3 \, \text{s}^{-1}$, and these values were used to classify the peak discharge in the anomaly assessment. The 25-year interval effectively represented the cold and warm Pacific Decadal Oscillation (PDO) pattern at the UCRW as well as how this atmospheric teleconnection affected local river discharge. Figure 9 shows the standardized anomaly time series of streamflow values in the Upper Columbia River. Classification of the annual events by the anomaly method resulted in 41 normal years, 37 wet years, and 41 dry years. Additionally, analysis of the anomaly values with a Mann–Kendall test yielded a negative trend of -0.08 (p value $= 0.02$; $\tau = -0.03$; $S = -209$), showing a dry tendency, which is consistent with the decline in open-water area and increase in woody/shrub vegetation during the 1984 to 2022 period.

The timing of the peak flow (Julian peak flow days) may be explained by the predominant PDO phase since 1903 (Table 2). Peaks flows tended to be late in the cold PDO (26, 22, and 15 June; as a consequence of colder air temperatures) and earlier during the warm PDO (20 and 16 June; due to higher air temperatures). However, regardless of the PDO phase, the
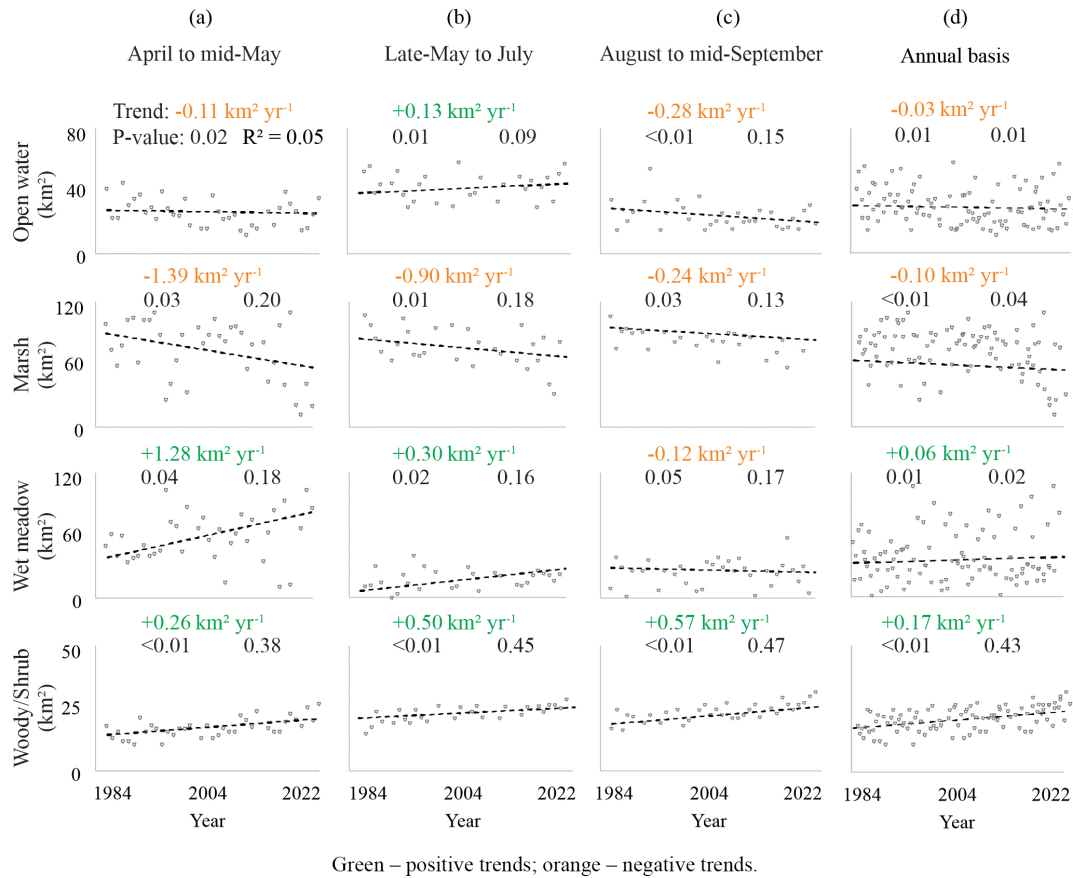
Figure 5. Trends in land cover extent during **(a)** April to mid-May, **(b)** late-May to July, **(c)** August to mid-September, and **(d)** on an annual basis (1984–2022).

Table 1. Historical and trends in hydroclimate variables (1984–2022).

Variable	Air temperature	Precipitation	Discharge		Water level	
			Annual	Peak flow	Annual	Peak level
Min	$-30.10\,°C$	$301.40\,mm$	$12.70\,m^3\,s^{-1}$	$283\,m^3\,s^{-1}$	$10.10\,cm$	$232.20\,cm$
Mean	$5.22\,°C$	$463.80\,mm$	$104.97\,m^3\,s^{-1}$	$428.18\,m^3\,s^{-1}$	$106.20\,cm$	$320.70\,cm$
Max	$25.70\,°C$	$641.40\,mm$	$748\,m^3\,s^{-1}$	$748\,m^3\,s^{-1}$	$421.40\,cm$	$421.40\,cm$
τ	0.02	-0.08	0.02	0.04	0.06	0.07
S	$1\,197\,480$	-62	$1\,382\,135$	25	$5\,098\,418$	45
p value	$0.02*$	$0.01*$	$< 0.01*$	$0.02*$	$< 0.01*$	$0.02*$
Slope	$0.02\,°C\,yr^{-1}$	$-0.75\,mm\,yr^{-1}$	$0.01\,m^3\,s^{-1}\,yr^{-1}$	$0.58\,m^3\,s^{-1}\,yr^{-1}$	$0.01\,cm\,yr^{-1}$	$0.63\,cm\,yr^{-1}$

* There is a significant temporal trend at the 5 % level. The variables listed in the table are as follows: Min – minimum; Max – maximum; S and τ – the trend (negative or positive); Slope – the 39-year increase or decrease in the variable; p value – the trend significance, where $p \leq 0.05$ denotes high significance.

Julian peak flow day is generally occurring earlier in the season (Table 2).

Table 2 summarizes the peak flow day for the Upper Columbia River and its duration since 1903. From 1903 to 1928, June 26 (Julian day 178) was found to be the approximate day of annual peak flow. From 2004 to 2022, peak flow occurred on average on 15 June (Julian day 169), 11 d earlier than in the past (i.e., 1903–1928). Peak flow duration also changed from an average of 22 d from 1903 to 1928 to 11 d after 2003. In contrast, if 1979–2003 is compared with 2004–2022 (the period of our remote sensing dataset), the peak flow was only earlier by 1 d, and its duration was shortened by 1 d. Thus, in the last century, the peak flows have gotten earlier in the season and the duration of peak flow has become shorter, resulting in a dryer floodplain during the summer growing season.

Table 2. Annual average peak flow day for each PDO group (1903–1928, 1929–1953, 1954–1978, 1979–2003, and 2004–2022) and the duration or length of each peak flow period.

	Julian peak flow day (date)	Var.	SD	Duration/Length of peak flow period (days)	Var.	SD
1903–1928	178 (26 June)	218	15	22	115	11
1929–1953	172 (20 June)	224	15	15	80	9
1954–1978	174 (22 June)	177	13	12	46	7
1979–2003	168 (16 June)	166	13	12	56	8
2004–2022	167 (15 June)	133	11	11	51	7

Var. – variance; SD – standard deviation
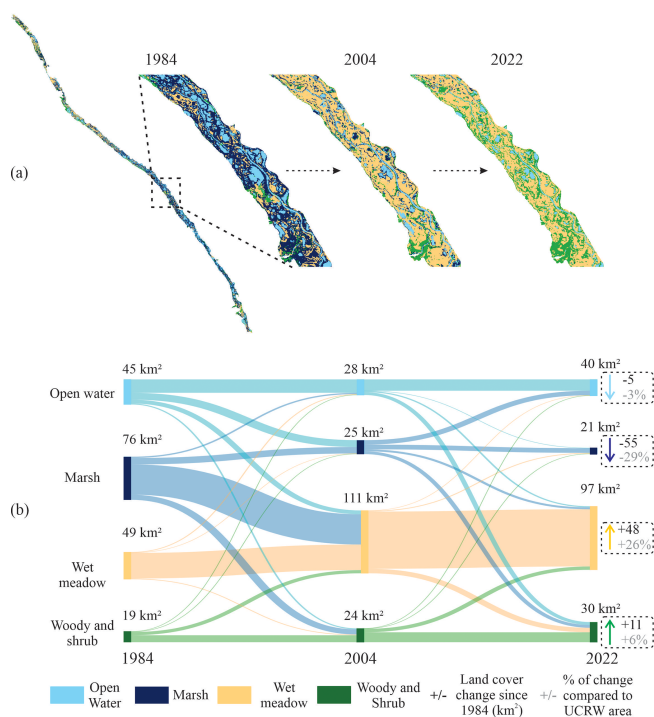
Figure 6. The Upper Columbia River floodplain distribution of land cover change from April to mid-May. The map insets in panel **(a)** indicate changes in land cover for sample regions. Panel **(b)** shows a Sankey diagram of the changes in land cover from 1984 to 2004 (left) and from 2004 to 2022 (right), the land cover change since 1984, and the percentage of change compared with the Columbia Wetlands area (188 km^2).
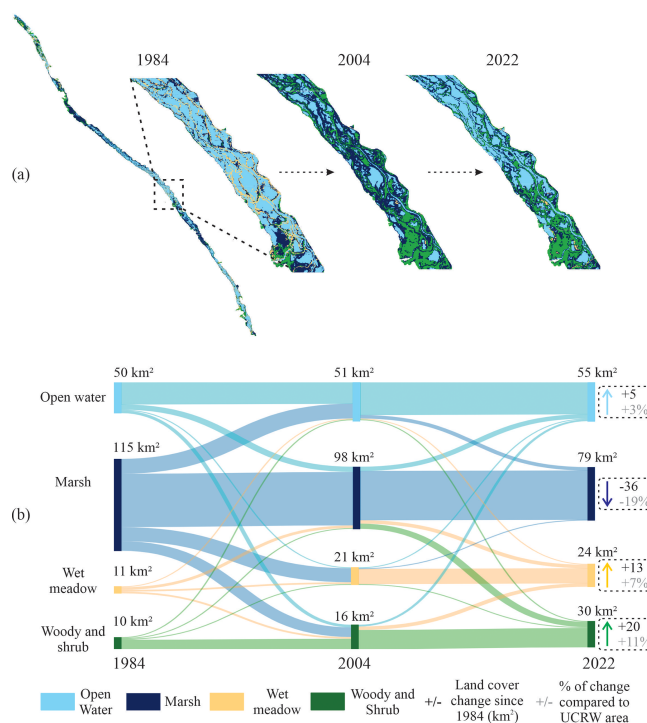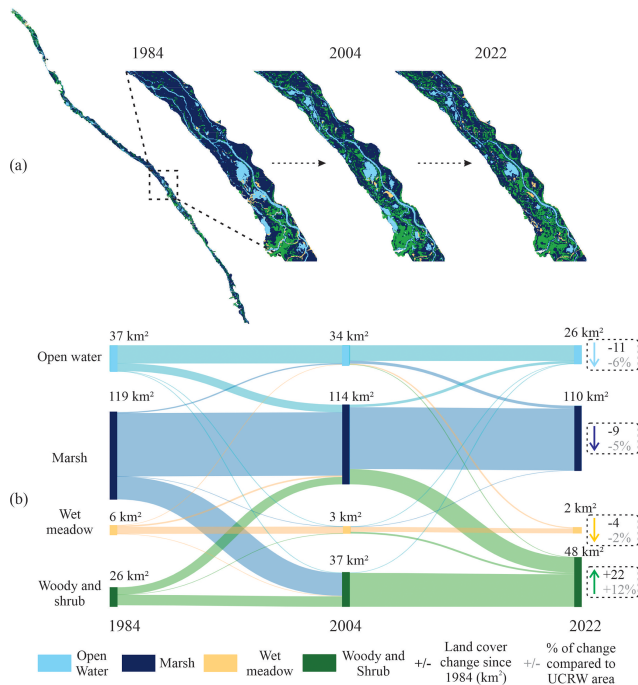

Figure 7. The Upper Columbia River floodplain distribution of land cover change from late-May to July. The map insets in panel **(a)** indicate changes in land cover for sample regions. Panel **(b)** shows a Sankey diagram of the changes in land cover from 1984 to 2004 (left) and from 2004 to 2022 (right), the land cover change since 1984, and the percentage of change compared with the Columbia Wetlands area (188 km^2).

The frequency analysis revealed that higher peaks appeared more frequently during 1903–1978, as the highest peak was 770 m^3 s^{-1}, while the lowest peak after 2003 was 305 m^3 s^{-1}, which was 233 % lower (Fig. 10a). Moreover, the daily discharge frequency (Fig. 10b) revealed that the 1903–1928 period had a higher discharge rate than post-2003 in terms of frequencies between 10 % and 60 %.

Figure 11a shows that baseflow has undergone a decrease (average of −1.5 %) from October to April since 1903 and that the peak flow hydrograph has a broader shape during the intervals from 1903 to 1928 and from 1929 to 1953, with a lower discharge, before becoming steeper with larger flows in a shorter amount of time. The positive trend in the recession constant coefficient over time, which is depicted in Fig. 11b, can also explain this pattern.

Figure 8. The Upper Columbia River floodplain distribution of land cover change from August to mid-September. The map insets in panel **(a)** indicate changes in land cover for sample regions. Panel **(b)** shows a Sankey diagram of the changes in land cover from 1984 to 2004 (left) and from 2004 to 2022 (right), the land cover change since 1984, and the percentage of change compared with the Columbia Wetlands area (188 km^2).
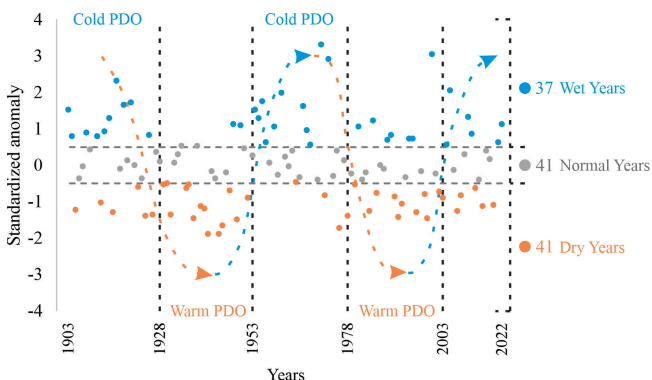
Figure 9. Standardized anomaly time series of annual peak flow of the Upper Columbia River at Nicholson (08NA002), British Columbia, Canada, and the predominant PDO phase in each 25-year period.

4 Discussion

4.1 Classification evaluation

The land cover classification used in this study was made possible by the utilization of various types of data for calibration and validation, resulting in an annual kappa aver-

age of 82 %, with higher precision during April to mid-May and the peak discharge period. At the beginning of the growing season (April to mid-May) the four classes (open water, marsh, wet meadow, and woody/shrub) were easier to distinguish. During the peak flow period, the floodplain surface is mostly covered by water, marsh, and woody vegetation, with a small area of wet meadow visible because the water levels were often so high that the dominant wetland meadow vegetation was covered. During the late summer (August to mid-September), there is higher greening in the marsh and woody/shrub vegetation, which creates some confusion between the vegetated classes. Moreover, marsh and wet meadow merge, which might contribute to the lower kappa value during the April to mid-May and August to mid-September periods. Furthermore, the years with additional available imagery (1984–1991, 2005, 2007, 2009, 2016, 2018, and 2022) for further training and validation were those for which RF performed better (average kappa of 0.84). This illustrates how an increase in high-quality training/validation sites improves the land cover classification.

In addition, based on the high correlation between river discharge and open water in the Upper Columbia River floodplain, the open-water area can be estimated from river discharge. This result is consistent with Hopkinson et al. (2020), who also found similar relationship over a smaller part of the UCRW (R^2 0.87). However, the moderate correlation (R^2 0.70) may be explained by the fact that the floodplain contains hundreds of wetlands that flood during peak flow and retain water during late-summer and spring. There is substantial variation, both spatially and temporally, in the flood depth, as the flood peak overtops the natural levees into all of the wetlands in some years, whereas water reaches into the wetlands through natural channels or gaps in the natural levees in other years. This results in a highly dynamic hydroperiod that influences vegetation communities in a wide range of ways.

Each year in early spring, the wetland water levels are at their lowest levels, when the Columbia River drops to 0.3 m (Environment Canada, 2022b), and there is a negative trend in open water during this season according to our results. If the open-water areas keep shrinking, marsh and wet meadows would be expected to reduce their area as well, and woody/shrub vegetation would be expected to encroach on the floodplain, which is what has been observed in all seasons. In contrast, when the flood pulse rises 2–4 m, much of the wet-meadow vegetation is covered by turbid floodwaters.

The UCRW has connected and non-connected wetlands, with both types experiencing variation in water levels and areal extent as the river rises and falls; however, more isolated wetland waterbodies may suffer permanent level and extent changes as a result of overbank flooding, slow drainage, loss to evapotranspiration (MacDonald and Chernos, 2020; Carli and Bayley, 2015), and climate change (Bürger et al., 2011; Carver, 2017; Jost et al., 2012). The aforementioned effects have primarily been seen between
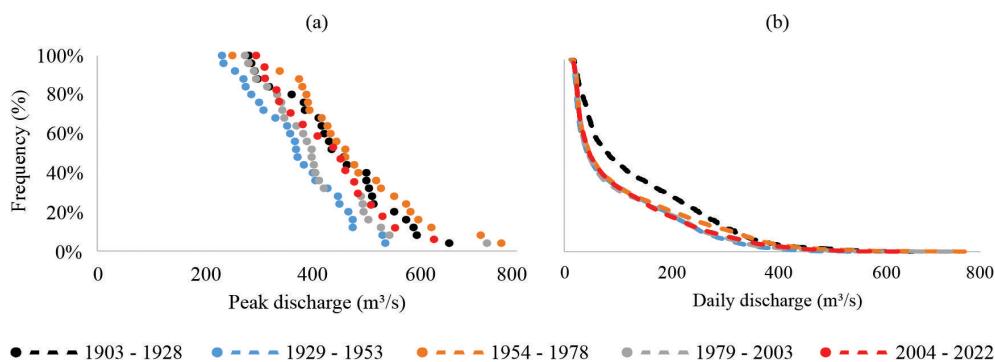
Figure 10. Frequency assessment of the Upper Columbia River peak **(a)** and daily discharge **(b)** from 1903 to 2022.
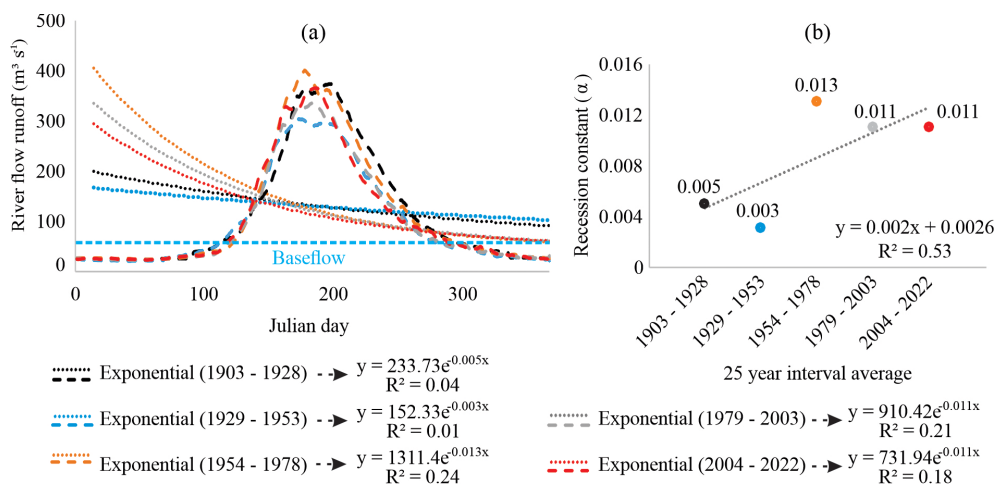
Figure 11. The **(a)** 25-year interval average river discharge hydrograph of the Upper Columbia River and **(b)** hydrograph recession constant tendency from the peak flow runoff (1903–1928, 1929–1953, 1954–1978, 1979–2003, and 2004–2022).

April and mid-May and between August to mid-September, when open water is shrinking and woody/shrub vegetation is encroaching on the floodplain.

4.2 Hydrometeorological changes in the Upper Columbia River basin

The positive trend in air temperature in the UCRW ($0.02\,°\text{C}\,\text{yr}^{-1}$) is consistent with an increase in global air temperatures during the same period (Hansen et al., 2010; Ohmura and Wild, 2002). Between 1900 and 1998, Western Canada warmed by $\sim 1\,°\text{C}$ (Zhang et al., 2000), and since the early 1960s, the trend on the eastern slopes of the Canadian Rocky Mountains has been warmer than the regional norm (2.6–3.6 °C) (Harder et al., 2015). The proportion of rainfall to total precipitation is predicted to increase as air temperatures increase, whereas the proportion of precipitation that falls as snow tends to decrease (Lapp et al., 2005). For the Canadian Rocky Mountains, trends in precipitation are mixed, with some studies reporting increasing trends of roughly 14 % during the period from 1948 to 2012 (Vincent et al., 2015) and other studies finding neither

trends nor change (Valeo et al., 2007) or a declining trend ($-0.75\,\text{mm}\,\text{yr}^{-1}$), the latter of which was observed in this study.

Streamflow is the basin-scale integrated response to these hydrometeorological changes, and in high-elevation headwater regions with limited meteorological monitoring, streamflow is a readily observable indicator that can be used to gauge hydroclimatic change (Harder et al., 2015). In the past century, several natural annual streamflows in the southern Canadian Rocky Mountains have decreased (Rood et al., 2005; Brahney et al., 2017), and peak streamflow events in some rivers have been observed to arrive earlier and with less flow volume, with late-summer flows dropping and winter flows rising (Rood et al., 2008). The positive trend in the annual basin discharge and peak flow was also seen in the UCRW, indicating that the peak flow had shifted to 11 d earlier and that the peak flow duration had decreased by 11 d (compared with pre-1928).

Although there is a positive trend in the peak discharge, the highest peak ($770\,\text{m}^3\,\text{s}^{-1}$) according to the frequency analysis was observed during 1903–1978. The lower peak dis-

charges post-1978 (compared with pre-1978) may be a result of the negative precipitation trend from 1984 to 2022. Furthermore, a negative trend was observed when it comes to daily discharge (which relates to the decrease in the baseflow since 1903), mostly at frequencies between 10 % and 60 %, referring to the start and end of the peak discharge, respectively. According to the historical analysis of the peak flow runoff hydrograph, the reduction of these flows (between 10 % and 60 %) typically leads to faster and higher peak discharge over fewer days; this is consistent with the positive tendency of the recession constant value and is also in accordance with Brahney et al. (2017), who observed an 11 % decline in river flow in the same area between 1947 and 2011, predominantly in late summer.

Another explanation for this pattern is through the anomaly assessment, which showed that dry or warm PDO phases are becoming drier, essentially post-1978, as per Newton et al. (2014), who observed a more severe dry PDO phase over the Canadian Cordillera since the 1970s. This suggests that the peak flow is shortening, whereas the magnitude of the discharge is increasing, causing higher discharges over fewer days and possibly impacting the water availability through the year (specifically in late summer), which relates to the downward annual basis open-water area trend. These results agree with Hopkinson et al. (2020), who used Landsat data to calculate the water extent and hydroperiod change from 1984 to 2019 in a portion of the Canadian Columbia Wetlands. They found a ∼ 16 % (or ∼ 3.5 % of the floodplain) reduction in the permanent water area extent, which is higher than the decrease in open water found in this research (−6 %) for the entire Columbia River valley over the year. Those aforementioned results are in accordance with other snow-driven montane ecosystems in Western Canada (Burn, 1994; Burn et al., 2004; Cutforth et al., 1999; Whitfield, 2001; Barnett et al., 2005; Stewart et al., 2005).

Under current and future climate change, earlier and faster snowmelt is expected, directly affecting the snow-accumulation- and melt-dominated watersheds (Steger et al., 2013; Pörtner et al., 2019). The positive trend in the air temperature is probably the cause of the earlier snowpack melt, which increases peak flow volumes while also shortening the duration (DeBeer et al., 2021). The rapid rise in the peak flow will enhance the open-water area during spring and summer, which (when combined with positive air temperature trends) may increase the evaporative demand, thereby impacting the amount of water that is lost to the atmosphere and whether or not these wetlands will shift into other land cover types, which can further enhance evapotranspiration (e.g., shrubs), essentially in late summer (Kienzle, 2006; Rasouli et al., 2022). The reduction in marsh and open water as well as the increase in wet-meadow and woody/shrub vegetation from August to mid-September are also reflected in this pattern.

4.3 Hydroclimatic trends as drivers of land cover change

Hydrological changes may be a key factor in this trend in the UCRW expansion of woody/shrub cover. Changes to the late-winter flow regime will affect ice formation and breakup, a fluvial geomorphic process that creates sites for seedling colonization by the riparian vegetation, encouraging clonal suckering (Rood et al., 2008). Woody/shrub vegetation is increasing because the land is drier for longer and, thus, the floodplain water table is lower, which leads to a drier root zone, allowing the spread of woody vegetation (Liu et al., 2022; Pellerin et al., 2016).

Regarding trends in woody encroachment, Barger et al. (2011) found positive trends of 0.8 % cover yr^{-1} in the Northern Rocky Mountains, USA, over a 30-year period. In the central region of the Rocky Mountains of Alberta, Glines (2012) observed a positive encroachment trend of 0.9 % cover yr^{-1} from 1952 to 2003. In Niwot Ridge, south of the Rocky Mountains, Formica et al. (2014) reported a positive woody encroachment trend of 0.2 % cover yr^{-1} over 62 years, which was the same rate found by Tape et al. (2006) in northern Alaska. The average annual positive trend (0.17 % km yr^{-1}) in woody/shrub encroachment in the our UCRW study is in accordance with other studies. Moreover, the woody ecotone advance has the potential to interfere with almost all regional components of the hydrological cycle, causing changes such as higher evapotranspiration by woodlands (Donohue et al., 2007), an increase in rainwater interception by the canopy trees (Owens et al., 2006), lower runoff (Bonan, 2008), and decreases in the groundwater recharge and streamflow (recharge below the rhizosphere) (Tennesen, 2008). The progression of wetland communities from herbaceous to woody plants is considered a natural succession (Vogl, 1969; Mitsch and Gosselink, 2000), although climate change has accelerated the woody ecotone encroachment in some mountain wetlands (Politti et al., 2014).

In addition to the possible effects of climate change, atmospheric teleconnection influences like El Niño and La Niña may significantly alter streamflow and impact land cover, as has been found in other studies across Western Canada (Gobena and Gan, 2006; Jacques et al., 2013; Fleming and Sauchyn, 2013; Chasmer and Hopkinson, 2017). El Niño appears to impact the UCRW, as the frequency of this phenomenon has increased since 1980s (Cai et al., 2021; Zhou et al., 2014), which may explain the predominantly dry pattern in this region (Yang et al., 2021) (number of years by anomaly: 13 normal years, 13 wet years, and 16 dry years), justifying the downward trend in open water on an annual basis.

The historical air temperature and precipitation record of the UCRW, resampled for El Niño and La Niña occurrences, can be used to overlay climate projections from general circulation models, which may result in more pronounced future changes to the region's precipitation and temperature.

Hydrol. Earth Syst. Sci., 28, 2203–2221, 2024

https://doi.org/10.5194/hess-28-2203-2024

According to the projections of the Special Report on Emissions Scenarios (Byers et al., 2022; IPCC, 2007) climate scenarios for the 2050s, the average annual precipitation of the Canadian Rocky Mountains could further decrease by about 5 %, while the average annual temperature could marginally increase by about 0.3 °C, under the potential combined impact of both climate change and El Niño. In contrast, based on the predictions of the Special Report on Emissions Scenarios for the 2050s (Byers et al., 2022; IPCC, 2007), La Niña years might see an additional 9 % increase in average precipitation with a concurrent 0.3 °C decrease in average temperature. The drying effect of climate change on the UCRW should be partly mitigated by a future La Niña year, but that effect could worsen in an El Niño year. These findings support those of Gobena and Gan (2006), who found that, in southwestern Canada, El Niño and La Niña occurrences cause large negative and positive streamflow anomalies, respectively.

In Western Canada, the Pacific North America (PNA) pattern is the active atmospheric teleconnection that has the greatest impact on the local climate and hydrology (Newton et al., 2014). The PNA pattern has a positive (i.e., relates to the Pacific warm episodes, El Niño, and characterized by above-average air temperatures) and a negative (i.e., associated with Pacific cold events, La Niña, marked by low-average air temperatures) phase (Lopez and Kirtman, 2019). The increased frequency of the positive phase of the PNA has been noticed over the years (Gan et al., 2023; Wang et al., 2017), and the main reason might be the continuous emissions of greenhouse warming (Cai et al., 2014). A more frequent positive phase of the PNA may lead to higher air temperatures, resulting in reductions in the seasonal snowpack (Mote et al., 2005; Brown and Robinson, 2011) and earlier spring runoff (Stewart et al., 2004).

Overall, the dominant changing seasonal hydrological processes within the UCRW include the following: shortening of the snowmelt period due to increasing air temperatures, which will boost the river discharge as well as the groundwater (essentially during the summer season); increasing and shortening of peak flows in summer due to the shortening period of snowmelt combined with higher-intensity rainfall and greater wetland flooding (Fig. 12b) (Musselman et al., 2018), which may also cause increased erosion in the uplands and siltation of the floodplain (Zhang et al., 2022); and, by late summer, water has moved through wetlands, causing them to dry, resulting in shrubification and enhanced water losses from evapotranspiration (Fig. 12c) (Li et al., 2020).

The UCRW has changed over the past 39 years as a result of the rise in air temperature and decrease in precipitation, which has caused significant changes in the floodplain. Remote sensing was used in this work to identify areas with low, moderate, and large shifts since 1984 and to evaluate the spatial distribution of land cover trends and changes. The results obtained illustrate the potential for the fusion of remote
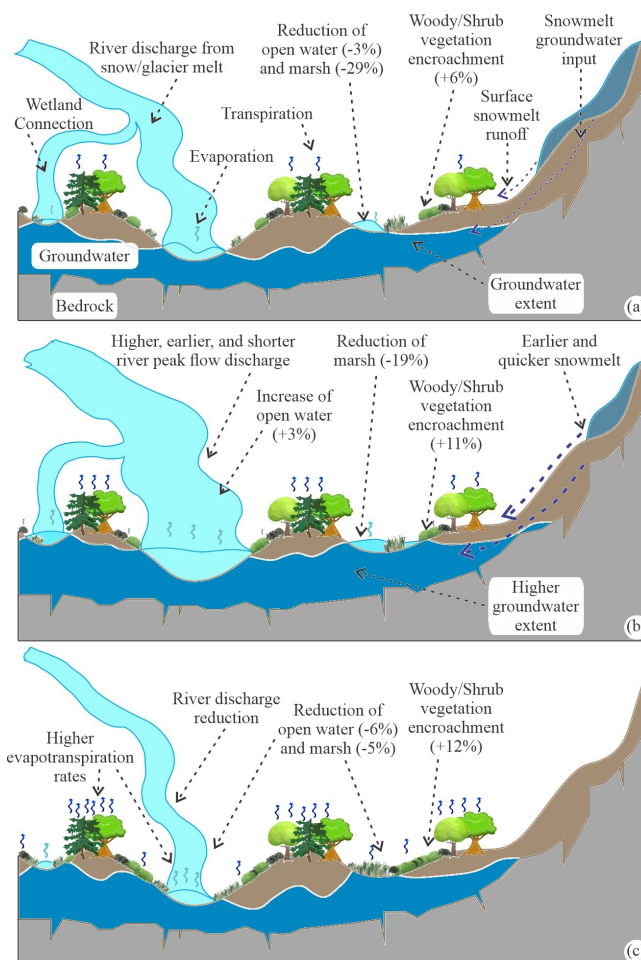
Figure 12. Updated conceptual understanding of the hydrological processes' conditions for the UCRW during **(a)** spring, **(b)** summer, and **(c)** late summer.

sensing and hydroclimatological data for the assessment of changing montane wetland environments.

5 Sources of uncertainty

Although the random forest algorithm demonstrated acceptable accuracy, several sources of uncertainty may be present with respect to the training and validation data sources as well as the spatial resolution of the Landsat imagery. It would be ideal to train and verify land cover classes using historical measured in situ field data. However, due to the constraints regarding temporal data availability, different remote sensing data sources were necessary for model calibration and validation in this historical land cover (LC) classification. The additional training pixels allocated using the higher-resolution dataset are at the beginning (1984–1991), in parts of the middle (2005, 2007, and 2009), and at the latter end of the time series (2016–2022), which tends to reduce the inaccuracies caused by the less-accurate data in other years (i.e., unchang-

ing pixels). A total of 60 unchanging pixels per LC class from the historical land cover classification of Canada (Hermosilla et al., 2022) (overall accuracy of 80 %) were used as the reference dataset for all years; therefore, any errors here could propagate into the UCRW LC classification. However, the distribution of the most reliable training and validation pixels (using higher-resolution datasets) over time has enabled accurate results, which, when compared to independent data sources, confirm the encroachment of woody/shrub vegetation (Politti et al., 2014; Primack, 2000; Theurillat and Guisan, 2001) and the reduction of open water during late summer (Rood et al., 2005; Kienzle, 2006; Rood et al., 2008) in montane wetlands.

Regarding the spatial resolution of the Landsat time series, 30 m is not the ideal resolution for classifying wetlands, as this habitat is typically mixed, with variable-width ecotones and vegetation inside open water and vice versa. In this study, the use of complementary remote sensing data sources has enabled temporal calibration and validation, but further enhancements may be possible via the addition of new data sources. For example, combining multispectral sensors with synthetic aperture radar (SAR) information may increase the accuracy up to 85 % (Loosvelt et al., 2012; Mahdianpari et al., 2017; Muro et al., 2020), as SAR is an effective tool to identify permanent open water (Montgomery et al., 2018).

6   Conclusion

In this study, we analyzed temporal trends and changes in land cover in the Upper Columbia River Wetlands using remote sensing and a random forest classification routine for a 39-year period. The classifier delivered a reasonable level of accuracy (kappa of 82 %). A total of 39 years of rising air temperature resulted in an increase in the Columbia River discharge. During the peak flow period, the open-water extent showed a positive tendency ($0.10\,\mathrm{km^2\,yr^{-1}}$); however, on an annual basis, the open-water area is declining ($-0.03\,\mathrm{km^2\,yr^{-1}}$). Furthermore, the peak flow occurs 1 d earlier now than ~ 40 years ago, and the peak flow duration has decreased by 1 d. However, since 2003, the peak flow has occurred 11 d earlier than 1903–1928, and its duration has decreased by 11 d, resulting in higher discharges in a shorter time. This also means that the summer period is drier and the land cover vegetation is subject to drier conditions. According to the anomaly assessment approach, dry years have been increasingly frequent since 1984.

Open-water areas of the floodplain have decreased in size during the April to mid-May period, while a large area of floodplain marsh has been replaced by wet meadow. In the same period (during the 39 years), shrub and woody vegetation increased by $11\,\mathrm{km^2}$. The peak flow period shows a decline in marsh regions and an increase in wet meadow, woody/shrub, and open water, the latter of which revealed a moderate increase. From August to mid-September, there was a decline in the amount of open water, marsh, and wet meadow but a significant increase in the amount of woody/shrub species.

Overall, the future of the Upper Columbia River Wetlands and their ecohydrological services are at risk due to the altered runoff regime that favors drying of the floodplain. Expansion of riparian shrub and treed ecotones are gradually replacing marsh and wet-meadow land covers commensurate with a reduction in permanent open-water area, which may lead to higher evapotranspiration, mainly during late summer, thus raising the potential for drought. While new floodplain riparian ecosystem habitats are being created, these come at the expense of lost open-water/aquatic habitat.

the Shuswap Band's Columbia Headwaters Aquatic Restoration Secwépemc Strategy (CHARS) project.

References

Amoros, C. and Bornette, G.: Connectivity and biocomplexity in waterbodies of riverine floodplains, Freshwater Biol., 47, 761–776, https://doi.org/10.1046/j.1365-2427.2002.00905.x, 2002.

Barger, N. N., Archer, S. R., Campbell, J. L., Huang, C. Y., Morton, J. A., and Knapp, A. K.: Woody plant proliferation in North American drylands: a synthesis of impacts on ecosystem carbon balance, J. Geophys. Res.-Biogeo., 116, G00K07, https://doi.org/10.1029/2010JG001506, 2011.

Barnett, T. P., Adam, J. C., and Lettenmaier, D. P.: Potential impacts of a warming climate on water availability in snow-dominated regions, Nature, 438, 303–309, https://doi.org/10.1038/nature04141, 2005.

Bayley, P. B.: Understanding large river: floodplain ecosystems, BioScience, 45, 153–158, https://doi.org/10.2307/1312554, 1995.

Bayley, S. E. and Guimond, J. K.: Effects of river connectivity on marsh vegetation community structure and species richness in montane floodplain wetlands in Jasper National Park, Alberta, Canada, Ecoscience, 15, 377–388, https://doi.org/10.2980/15-3-3084, 2008.

Bayley, S. E. and Guimond, J. K.: Aboveground biomass and nutrient limitation in relation to river connectivity in montane floodplain marshes, Wetlands, 29, 1243–1254, https://doi.org/10.1672/08-227.1, 2009.

BC Government: Digital Air Photos of B.C., Province of British Columbia, https://www2.gov.bc.ca/gov/content/data/geographic-data-services/digital-imagery/air-photos (last access: 15 January 2022), 2022.

Berhail, S., Ouerdachi, L., and Boutaghane, H.: The use of the recession index as indicator for components of flow, Energy Proced., 18, 741–750, https://doi.org/10.1016/j.egypro.2012.05.090, 2012.

Bonan, G. B.: Forests and climate change: forcings, feedbacks, and the climate benefits of forests, Science, 320, 1444–1449, https://doi.org/10.1126/science.1155121, 2008.

Brahney, J., Weber, F., Foord, V., Janmaat, J., and Curtis, P. J.: Evidence for a climate-driven hydrologic regime shift in the Canadian Columbia Basin, Can. Water Resour. J., 42, 179–192, https://doi.org/10.1080/07011784.2016.1268933, 2017.

Breiman, L.: Random forests, Mach. Learn., 45, 5–32, https://doi.org/10.1023/A:1010933404324, 2001.

Brown, R. D. and Robinson, D. A.: Northern Hemisphere spring snow cover variability and change over 1922–2010 including an assessment of uncertainty, The Cryosphere, 5, 219–229, https://doi.org/10.5194/tc-5-219-2011, 2011.

Brutsaert, W. and Nieber, J. L.: Regionalized drought flow hydrographs from a mature glaciated plateau, Water Resour. Res., 13, 637–643, https://doi.org/10.1029/WR013i003p00637, 1977.

Burn, D. H.: Hydrologic effects of climatic change in west-central Canada, J. Hydrol., 160, 53–70, https://doi.org/10.1016/0022-1694(94)90033-7, 1994.

Burn, D. H., Abdul Aziz, O. I., and Pietroniro, A.: A comparison of trends in hydrological variables for two watersheds in the Mackenzie River Basin, Can. Water Resour. J., 29, 283–298, https://doi.org/10.4296/cwrj283, 2004.

Bürger, G., Schulla, J., and Werner, A. T.: Estimates of future flow, including extremes, of the Columbia River headwaters, Water Resour. Res., 47, W10520, https://doi.org/10.1029/2010WR009716, 2011.

Byers, E., Krey, V., Kriegler, E., Riahi, K., Schaeffer, R., Kikstra, J., Lamboll, R., Nicholls, Z., Sandstad, M., Smith, C., van der Wijst, K., Lecocq, F., Portugal-Pereira, J., Saheb, Y., Stromann, A., Winkler, H., Auer, C., Brutschin, E., Lepault, C., Müller-Casseres, E., Gidden, M., Huppmann, D., Kolp, P., Marangoni, G., Werning, M., Calvin, K., Guivarch, C., Hasegawa, T., Peters, G., Steinberger, J., Tavoni, M., van Vuuren, D., Al -Khourdajie, A., Forster, P., Lewis, J., Meinshausen, M., Rogelj, J., Samset, B., and Skeie, R.: AR6 scenarios database, Zenodo [data set], https://doi.org/10.5281/zenodo.7197970, 2022.

Cai, W., Borlace, S., Lengaigne, M., Rensch, P. V., Collins, M., Vecchi, G., Timmermann, A., Santoso, A., McPhaden, M. J., Wu, L., England, M. H., Wang, G., Guiyardy, E., and Jin, F. F.: Increasing frequency of extreme El Niño events due to greenhouse warming, Nat. Clim. Change, 4, 111–116, https://doi.org/10.1038/nclimate2100, 2014.

Cai, W., Santoso, A., Collins, M., Dewitte, B., Karamperidou, C., Kug, J.-S., Lengaigne, M., McPhaden, M. J., Stuecker, M. F., Taschetto, A. S., Timmermann, A., Wu, L., Yeh, S.-W., Wang, G., Ng, B., Jia, F., Yang, Y., Ying, J., Zheng, X.-T., Bayr, T., Brown, J.R., Capotondi, A., Cobb, K. M., Gan, B., Geng, T., Ham, Y.-G., Jin, F.-F., Jo, H.-S., Li, X., Lin, X., McGregor, S., Park, J.-H., Stein, K., Yang, K., Zhang, L., and Zhong, W.: Changing El Niño–Southern oscillation in a warming climate, Nat. Rev. Earth Environ., 2, 628–644, https://doi.org/10.1038/s43017-021-00199-z, 2021.

Carli, C. M. and Bayley, S. E.: River connectivity and road crossing effects on floodplain vegetation of the upper Columbia River, Canada, Ecoscience, 22, 97–107, https://doi.org/10.1080/11956860.2015.1121705, 2015.

Carver, M.: Water monitoring and climate change in the upper Columbia Basin: Summary of current status and opportunities, Golden, BC, V0A 1H0: Columbia Basin Trust, https://ourtrust.org/wp-content/uploads/downloads/WaterMonitoringandClimateChange_FullReport_2017_FINAL_Web-5.pdf (last access: 26 November 2022), 2017.

Chasmer, L., Cobbaert, D., Mahoney, C., Millard, K., Peters, D., Devito, Brisco, B., Hopkinson , C., Merchant, M., Montgomery, J. , Nelson, K., and Niemann, O.: Remote Sensing of Boreal Wetlands 1: Data Use for Policy and Management, Remote Sensing, 12, 1320, https://doi.org/10.3390/rs12081320, 2020.

Congalton, R. G. and Green, K.: Assessing the accuracy of remotely sensed data: principles and practices, CRC Press, https://doi.org/10.1201/9780429052729, 2019.

Cooper, D. J., Chimner, R. A., and Merritt, D. M.: Western Mountain wetlands University of California Press, Berkeley, CA, USA, 313–328, https://books.google.com.br/books?hl=pt-BR&lr=&id=hvS5xljxuL4C&oi=fnd&pg=PA313&dq=Western+Mountain+wetlands+University+of+California+Press,+Berkeley,+CA,+USA&ots=7_AX5blENY&sig=EKSD2zO3BHev-cPzyf90GD5aFv8#v=onepage&q&f=false (last access: 26 November 2022), 2012.

Cooper, D. J., Kaczynski, K. M., Sueltenfuss, J., Gaucherand, S., and Hazen, C.: Mountain wetland restoration: the role of hydrologic regime and plant introductions after 15 years in the Colorado Rocky Mountains, USA, Ecol. Eng., 101, 46–59, https://doi.org/10.1016/j.ecoleng.2017.01.017, 2017.

Chasmer, L. and Hopkinson, C.: Threshold loss of discontinuous permafrost and landscape evolution, Glob. Change Biol., 23, 2672–2686, https://doi.org/10.1111/gcb.13537, 2017.

Cutforth, H. W., McConkey, B. G., Woodvine, R. J., Smith, D. G., Jefferson, P. G., and Akinremi, O. O.: Climate change in the semiarid prairie of southwestern Saskatchewan: Late winter–early spring, Can. J. Plant Sci., 79, 343–350, https://doi.org/10.4141/P98-137, 1999.

DeBeer, C. M., Wheater, H. S., Carey, S. K., and Chun, K. P.: Recent climatic, cryospheric, and hydrological changes over the interior of western Canada: a review and synthesis, Hydrol. Earth Syst. Sci., 20, 1573–1598, https://doi.org/10.5194/hess-20-1573-2016, 2016.

DeBeer, C. M., Wheater, H. S., Pomeroy, J. W., Barr, A. G., Baltzer, J. L., Johnstone, J. F., Turetsky, M. R., Stewart, R. E., Hayashi, M., van der Kamp, G., Marshall, S., Campbell, E., Marsh, P., Carey, S. K., Quinton, W. L., Li, Y., Razavi, S., Berg, A., McDonnell, J. J., Spence, C., Helgason, W. D., Ireson, A. M., Black, T. A., Elshamy, M., Yassin, F., Davison, B., Howard, A., Thériault, J. M., Shook, K., Demuth, M. N., and Pietroniro, A.: Summary and synthesis of Changing Cold Regions Network (CCRN) research in the interior of western Canada – Part 2: Future change in cryosphere, vegetation, and hydrology, Hydrol. Earth Syst. Sci., 25, 1849–1882, https://doi.org/10.5194/hess-25-1849-2021, 2021.

Díaz, S., Demissew, S., Carabias, J., Joly, C., Lonsdale, M., Ash, N., Larigauderie, A., Adhikari, J. R., Arico, S., Báldi, A., Bartuska, A., Baste, I. A., Bilgin, A., Brondizio, E., Chan, K. M. A., Figueroa, V. E., Duraiappah, A., Fischer, M., Hill, R., Koetz, T., Leadley, P., Lyver, P., Mace, G. M., Martin-Lopez, B., Okumura, M., Pacheco, D., Pascual, U., Pérez, E. S., Reyers, B., Roth, E., Saito, O., Scholes, R. J., Sharma, N., Tallis, H., Thaman, R., Watson, R., Yahara, T., Hamid, Z. A., Akosim, C., Al-Hafedh, Y., Allahverdiyev, R., Amankwah, E., Asah, T. S., Asfaw, Z., Bartus, G., Brooks, A. L., Caillaux, J., Dalle, G., Darnaedi, D., Driver, A., Erpul, G., Escobar-Eyzaguirre, P., Failler, P., Fouda, A. M. M., Fu, B., Gundimeda, H., Hashimoto, S., Homer, F., Lavorel, S., Lichtenstein, G., Mala, W. A., Mandivenyi, W., Matczak, P., Mbizvo, C., Mehrdadi, M., Metzger, J. P., Mikissa, J. B., Moller, H., Mooney, H. A., Mumby, P., Nagendra, H., Nesshover, C., Oteng-Yeboah, A. A., Pataki, G., Roué, M., Rubis, J., Schultz, M., Smith, P., Sumaila, R., Takeuchi, K., Thomas, S., Verma, M., Yeo-Chang, Y., and Zlatanova, D.: The IPBES Conceptual Framework – connecting nature and people, Curr. Opin. Sust., 14, 1–16, https://doi.org/10.1016/j.cosust.2014.11.002, 2015.

Donohue, R. J., Roderick, M. L., and McVicar, T. R.: On the importance of including vegetation dynamics in Budyko's hydrological model, Hydrol. Earth Syst. Sci., 11, 983–995, https://doi.org/10.5194/hess-11-983-2007, 2007.

Edwards, T. W., Birks, S. J., Luckman, B. H., and MacDonald, G. M.: Climatic and hydrologic variability during the past millennium in the eastern Rocky Mountains and northern Great Plains of western Canada, Quaternary Res., 70, 188–197, https://doi.org/10.1016/j.yqres.2008.04.013, 2008.

Environment Canada: Historical climate data, Environment Canada, https://climate.weather.gc.ca/historical_data/search_historic_data_e.html (last access: 3 November 2022), 2022a.

Environment Canada: HYDAT database, Environment Canada, https://wateroffice.ec.gc.ca/search/historical_e.html (last access: 4 November 2022), 2022b.

Fleming, S. W. and Sauchyn, D. J.: Availability, volatility, stability, and teleconnectivity changes in prairie water supply from Canadian Rocky Mountain sources over the last millennium, Water Resour. Res., 49, 64–74, https://doi.org/10.1029/2012WR012831, 2013.

Formica, A., Farrer, E. C., Ashton, I. W., and Suding, K. N.: Shrub expansion over the past 62 years in Rocky Mountain alpine tundra: possible causes and consequences, Arct. Antarct. Alp. Res., 46, 616–631, https://doi.org/10.1657/1938-4246-46.3.616, 2014.

Foster, L. M., Bearup, L. A., Molotch, N. P., Brooks, P. D., and Maxwell, R. M.: Energy budget increases reduce mean streamflow more than snow–rain transitions: Using integrated modeling to isolate climate change impacts on Rocky Mountain hydrology, Environ. Res. Lett., 11, 044015, https://doi.org/10.1088/1748-9326/11/4/044015, 2016.

Gan, R., Liu, Q., Huang, G., Hu, K., and Li, X.: Greenhouse warming and internal variability increase extreme and central Pacific El Niño frequency since 1980, Nat. Commun., 14, 394, https://doi.org/10.1038/s41467-023-36053-7, 2023.

Genz, F. and Luz, L. D.: Distinguishing the effects of climate on discharge in a tropical river highly impacted by large dams, Hydrolog. Sci. J., 57, 1020–1034, https://doi.org/10.1080/02626667.2012.690880, 2012.

Glines, L. M.: Woody plant encroachment into grasslands within the Red Deer River drainage, Alberta, University of Alberta, https://doi.org/10.7939/R33H5V, 2012.

Gobena, A. K. and Gan, T. Y.: Low-frequency variability in Southwestern Canadian stream flow: links with large-scale climate anomalies, Int. J. Climatol., 26, 1843–1869, https://doi.org/10.1002/joc.1336, 2006.

Hansen, J., Ruedy, R., Sato, M., and Lo, K.: Global surface temperature change, Rev. Geophys., 48, 1–29, https://doi.org/10.1029/2010RG000345, 2010.

Harder, P., Pomeroy, J. W., and Westbrook, C. J.: Hydrological resilience of a Canadian Rockies headwaters basin subject to changing climate, extreme weather, and forest management, Hydrol. Process., 29, 3905–3924, https://doi.org/10.1002/hyp.10596, 2015.

Hathaway, J. M., Westbrook, C. J., Rooney, R. C., Petrone, R. M., and Langs, L. E.: Quantifying relative contributions of source waters from a subalpine wetland to

downstream water bodies, Hydrol. Process., 36, e14679, https://doi.org/10.1002/hyp.14679, 2022.

Hermosilla, T., Wulder, M. A., White, J. C., and Coops, N. C.: Land cover classification in an era of big and open data: Optimizing localized implementation and training data selection to improve mapping outcomes, Remote Sens. Environ., 268, 112780, https://doi.org/10.1016/j.rse.2021.112780, 2022.

Hernandez, M. E. and Mitsch, W. J.: Influence of hydrologic pulses, flooding frequency, and vegetation on nitrous oxide emissions from created riparian marshes, Wetlands, 26, 862–877, https://doi.org/10.1672/0277-5212(2006)26[862:IOHPFF]2.0.CO;2, 2006.

Hersbach, H., Bell, B., Berrisford, P., Hirahara, S., Horányi, A., Muñoz-Sabater, J., Nicolas, J., Peubey, C., Radu, R., Schepers, D., Simmons, A., Soci, C., Abdalla, S., Abellan, X., Balsamo, G., Bechtold, P., Biavati, G., Bidlot, J., Bonavita, M., De Chiara, G., Dahlgren, P., Dee, D., Diamantakis, M., Dragani, R., Flemming, J., Forbes, R., Fuentes, M., Geer, A., Haimberger, L., Healy, S., Hogan, R. J., Hólm, E., Janisková, M., Keeley, S., Laloyaux, P., Lopez, P., Lupu, C., Radnoti, G., de Rosnay, P., Rozum, I., Vamborg, F., Villaume, S., and Thépaut, J.-N.: The ERA5 global reanalysis, Q. J. Roy. Meteor. Soc., 146, 1999–2049, https://doi.org/10.1002/qj.3803, 2020.

Hopkinson, C. and Young, G. J.: The effect of glacier wastage on the flow of the Bow River at Banff, Alberta, 1951–1993, Hydrol. Process., 12, 1745–1762, https://doi.org/10.1002/(SICI)1099-1085(199808/09)12:10/11<1745::AID-HYP692>3.0.CO;2-S, 1998.

Hopkinson, C., Fuoco, B., Grant, T., Bayley, S. E., Brisco, B., and MacDonald, R.: Wetland Hydroperiod Change Along the Upper Columbia River Floodplain, Canada, 1984 to 2019, Remote Sensing, 12, 4084, https://doi.org/10.3390/rs12244084, 2020.

Hrach, D. M., Petrone, R. M., Green, A., and Khomik, M.: Analysis of growing season carbon and water fluxes of a subalpine wetland in the Canadian Rocky Mountains: implications of shade on ecosystem water use efficiency, Hydrol. Process., 36, e14425, https://doi.org/10.1002/hyp.14425, 2022.

Hughes, F. M.: Floodplain biogeomorphology, Prog. Phys. Geog., 21, 501–529, https://doi.org/10.1177/030913339702100402, 1997.

Hussain, M. and Mahmud, I.: pyMannKendall: a python package for non parametric Mann Kendall family of trend tests, Journal of Open Source Software, 4, 1556, https://doi.org/10.21105/joss.01556, 2019.

Inglada, J., Vincent, A., Arias, M., Tardy, B., Morin, D., and Rodes, I.: Operational high resolution land cover map production at the country scale using satellite image time series, Remote Sensing, 9, 95, https://doi.org/10.3390/rs9010095 2017.

IPCC: Climate Change, Intergovernmental Panel on Climate Change Fourth Assessment Report, https://doi.org/10.1029/2005JD006713, 2007.

Jacques, J. M. S., Lapp, S. L., Zhao, Y., Barrow, E. M., and Sauchyn, D. J.: Twenty-first century central Rocky Mountain river discharge scenarios under greenhouse forcing, Quatern. Int., 310, 34–46, https://doi.org/10.1016/j.quaint.2012.06.023, 2013.

Jost, G., Moore, R. D., Menounos, B., and Wheate, R.: Quantifying the contribution of glacier runoff to streamflow in the upper Columbia River Basin, Canada, Hydrol. Earth Syst. Sci., 16, 849–860, https://doi.org/10.5194/hess-16-849-2012, 2012.

Ju, J. and Masek, J. G.: The vegetation greenness trend in Canada and US Alaska from 1984–2012 Landsat data, Remote Sens. Environ., 176, 1–16, https://doi.org/10.1016/j.rse.2016.01.001, 2016.

Junk, W. J., Bayley, P. B., and Sparks, R. E.: The flood pulse concept in river-floodplain systems, Canadian Special Publication of Fisheries and Aquatic Sciences, 106, 110–127, 1989.

Kendall, M. G.: Rank correlation methods, London: Griffin, 160 pp., 1948.

Kienzle, S. W.: The use of the recession index as an indicator for streamflow recovery after a multi-year drought, Water Resour. Manag., 20, 991–1006, https://doi.org/10.1007/s11269-006-9019-1, 2006.

Lacoul, P. and Freedman, B.: Environmental influences on aquatic plants in freshwater ecosystems, Environ. Rev., 14, 89–136, https://doi.org/10.1139/A06-001, 2006.

Lapp, S., Byrne, J., Townshend, I., and Kienzle, S.: Climate warming impacts on snowpack accumulation in an alpine watershed, Int. J. Climatol., 25, 521–536, https://doi.org/10.1002/joc.1140, 2005.

Leppi, J. C., DeLuca, T. H., Harrar, S. W., and Running, S. W.: Impacts of climate change on August stream discharge in the Central-Rocky Mountains, Climatic Change, 112, 997–1014, https://doi.org/10.1007/s10584-011-0235-1, 2012.

Li, Z., Wang, S., and Li, J.: Spatial variations and long-term trends of potential evaporation in Canada, Sci. Rep., 10, 1–14, https://doi.org/10.1038/s41598-020-78994-9, 2020.

Linsley, B. K., Wu, H. C., Dassié, E. P., and Schrag, D. P.: Decadal changes in South Pacific sea surface temperatures and the relationship to the Pacific decadal oscillation and upper ocean heat content, Geophys. Res. Lett., 42, 2358–2366, https://doi.org/10.1002/2015GL063045, 2015.

Liu, Y. F., Cui, Z., Huang, Z., López-Vicente, M., Zhao, J., Ding, L., and Wu, G. L.: Shrub encroachment in alpine meadows increases the potential risk of surface soil salinization by redistributing soil water, Catena, 219, 106593, https://doi.org/10.1016/j.catena.2022.106593, 2022.

Loeffler, J., Anschlag, K., Baker, B., Finch, O. D., Diekkrueger, B., Wundram, D., Schröder, Pape, B., R., and Lundberg, A.: Mountain ecosystem response to global change, Erdkunde, 65, 189–213, https://www.jstor.org/stable/23030665 (last access: 25 November 2022), 2011.

Loosvelt, L., Peters, J., Skriver, H., De Baets, B., and Verhoest, N. E.: Impact of reducing polarimetric SAR input on the uncertainty of crop classifications based on the random forests algorithm, IEEE T. Geosci. Remote, 50, 4185–4200, https://doi.org/10.1109/TGRS.2012.2189012, 2012.

Lopez, H. and Kirtman, B. P.: ENSO influence over the Pacific North American sector: Uncertainty due to atmospheric internal variability, Clim. Dynam., 52, 6149–6172, https://doi.org/10.1007/s00382-018-4500-0, 2019.

Lottig, N. R., Buffam, I., and Stanley, E. H.: Comparisons of wetland and drainage lake influences on stream dissolved carbon concentrations and yields in a north temperate lake-rich region, Aquat. Sci., 75, 619–630, https://doi.org/10.1007/s00027-013-0305-8, 2013.

McCaffrey, D. R. and Hopkinson, C.: Modelling Watershed-Scale Historic Change in the Alpine Treeline Ecotone Us-

ing Random Forest, Can. J. Remote Sens., 46, 715–732, https://doi.org/10.1080/07038992.2020.1865792, 2020.

MacDonald, R. and Chernos, M.: Hydrological Assessment of the Upper Columbia River Watershed, MacHydro Consultants Ltd., Cranbrook, BC, Canada, 64, https://wetlandstewards.eco/wp-content/uploads/2020/02/CWSP_Hydrology-CV-Watershed-Report_Final-Jan-31-2020.pdf (last access: 30 November 2022), 2020.

MacDonald, G. M., Edwards, T. W., Moser, K. A., Pienitz, R., and Smol, J. P.: Rapid response of treeline vegetation and lakes to past climate warming, Nature, 361, 243–246, https://doi.org/10.1038/361243a0, 1993.

Mahdianpari, M., Salehi, B., Mohammadimanesh, F., and Brisco, B.: An assessment of simulated compact polarimetric SAR data for wetland classification using random forest algorithm, Can. J. Remote Sens., 43, 468–484, https://doi.org/10.1080/07038992.2017.1381550, 2017.

Mann, H. B.: Nonparametric tests against trend. Econometrica, Journal of the Econometric Society, 13, 245–259, 1945.

Mantua, N. J. and Hare, S. R.: The Pacific decadal oscillation, J. Oceanogr., 58, 35–44, https://doi.org/10.1023/A:1015820616384, 2002.

Marshall, S. J.: Meltwater run-off from Haig Glacier, Canadian Rocky Mountains, 2002–2013, Hydrol. Earth Syst. Sci., 18, 5181–5200, https://doi.org/10.5194/hess-18-5181-2014, 2014.

Menze, B. H., Kelm, B. M., Masuch, R., Himmelreich, U., Bachert, P., Petrich, W., and Hamprecht, F. A.: A comparison of random forest and its Gini importance with standard chemometric methods for the feature selection and classification of spectral data, BMC Bioinformatics, 10, 1–16, https://doi.org/10.1186/1471-2105-10-213, 2009.

Millar, D. J., Cooper, D. J., and Ronayne, M. J.: Groundwater dynamics in mountain peatlands with contrasting climate, vegetation, and hydrogeological setting, J. Hydrol., 561, 908–917, https://doi.org/10.1016/j.jhydrol.2018.04.050, 2018.

Millard, K. and Richardson, M.: On the importance of training data sample selection in random forest image classification: A case study in peatland ecosystem mapping, Remote Sensing, 7, 8489–8515, https://doi.org/10.3390/rs70708489, 2015.

Mitch, W. J. and Gosselink, J. G.: Wetlands, John Wiley & Sons, 3rd edn., ISBN 9780471699675, 2000.

Montgomery, J. S., Hopkinson, C., Brisco, B., Patterson, S., and Rood, S. B.: Wetland hydroperiod classification in the western prairies using multitemporal synthetic aperture radar, Hydrol. Process., 32, 1476–1490, https://doi.org/10.1002/hyp.11506, 2018.

Mote, P. W., Hamlet, A. F., Clark, M. P., and Lettenmaier, D. P.: Declining mountain snowpack in western North America, B. Am. Meteorol. Soc., 86, 39–50, https://doi.org/10.1175/BAMS-86-1-39, 2005.

Muro, J., Varea, A., Strauch, A., Guelmami, A., Fitoka, E., Thonfeld, F., Thonfeld, B. Diekkrüger, and Waske, B.: Multitemporal optical and radar metrics for wetland mapping at national level in Albania, Heliyon, 6, e04496, https://doi.org/10.1016/j.heliyon.2020.e04496, 2020.

Musselman, K. N., Lehner, F., Ikeda, K., Clark, M. P., Prein, A. F., Liu, C., Barlage, M., and Rasmussen, R.: Projected increases and shifts in rain-on-snow flood risk over western North America, Nat. Clim. Change, 8, 808–812, https://doi.org/10.1038/s41558-018-0236-4, 2018.

Newton, B. W., Prowse, T. D., and Bonsal, B. R.: Evaluating the distribution of water resources in western Canada using synoptic climatology and selected teleconnections. Part 2: Summer season, Hydrol. Process., 28, 4235–4249, https://doi.org/10.1002/hyp.10235, 2014.

Ohmura, A. and Wild, M.: Is the hydrological cycle accelerating?, Science, 298, 1345–1346, https://doi.org/10.1126/science.1078972, 2002.

Owens, M. K., Lyons, R. K., and Alejandro, C. L.: Rainfall partitioning within semiarid juniper communities: effects of event size and canopy cover, Hydrol. Process., 20, 3179–3189, https://doi.org/10.1002/hyp.6326, 2006.

Pellerin, S., Lavoie, M., Boucheny, A., Larocque, M., and Garneau, M.: Recent vegetation dynamics and hydrological changes in bogs located in an agricultural landscape, Wetlands, 36, 159–168, https://doi.org/10.1007/s13157-015-0726-3, 2016.

Pelletier, C., Valero, S., Inglada, J., Champion, N., and Dedieu, G.: Assessing the robustness of Random Forests to map land cover with high resolution satellite image time series over large areas, Remote Sens. Environ., 187, 156–168, https://doi.org/10.1016/j.rse.2016.10.010, 2016.

Politti, E., Egger, G., Angermann, K., Rivaes, R., Blamauer, B., Klösch, M., Tritthart, M., and Habersack, H.: Evaluating climate change impacts on Alpine floodplain vegetation, Hydrobiologia, 737, 225–243, https://doi.org/10.1007/s10750-013-1801-5, 2014.

Pörtner, H. O., Roberts, D. C., Masson-Delmotte, V., Zhai, P., Tignor, M., Poloczanska, E., and Weyer, N. M.: The ocean and cryosphere in a changing climate, IPCC Special Report on the Ocean and Cryosphere in a Changing Climate, https://doi.org/10.1017/9781009157964, 2019.

Primack, A. G.: Simulation of climate-change effects on riparian vegetation in the Pere Marquette River, Michigan, Wetlands, 20, 538–547, https://doi.org/10.1672/0277-5212(2000)020<0538:SOCEOR>2.0.CO;2, 2000.

Rasouli, K., Pomeroy, J. W., and Whitfield, P. H.: The sensitivity of snow hydrology to changes in air temperature and precipitation in three North American headwater basins, J. Hydrol., 606, 127460, https://doi.org/10.1016/j.jhydrol.2022.127460, 2022.

Ray, A. M., Sepulveda, A. J., Irvine, K. M., Wilmoth, S. K., Thoma, D. P., and Patla, D. A.: Wetland drying linked to variations in snowmelt runoff across Grand Teton and Yellowstone national parks, Sci. Total Environ., 666, 1188–1197, https://doi.org/10.1016/j.scitotenv.2019.02.296, 2019.

Rodrigues, I. S.: GEE-RF-LC-code: GEE-RF-code, Zenodo [code], https://doi.org/10.5281/zenodo.11159362, 2024.

Rood, S. B., Samuelson, G. M., Weber, J. K., and Wywrot, K. A.: Twentieth-century decline in streamflows from the hydrographic apex of North America, J. Hydrol., 306, 215–233, https://doi.org/10.1016/j.jhydrol.2004.09.010, 2005.

Rood, S. B., Pan, J., Gill, K. M., Franks, C. G., Samuelson, G. M., and Shepherd, A.: Declining summer flows of Rocky Mountain rivers: Changing seasonal hydrology and probable impacts on floodplain forests, J. Hydrol., 349, 397–410, https://doi.org/10.1016/j.jhydrol.2007.11.012, 2008.

Schnorbus, M., Werner, A., and Bennett, K.: Impacts of climate change in three hydrologic regimes in British

Hydrol. Earth Syst. Sci., 28, 2203–2221, 2024

https://doi.org/10.5194/hess-28-2203-2024

Columbia, Canada, Hydrol. Process., 28, 1170–1189, https://doi.org/10.1002/hyp.9661, 2014.

Sparks, R. E., Bayley, P. B., Kohler, S. L., and Osborne, L. L.: Disturbance and recovery of large floodplain rivers, Environ. Manage., 14, 699–709, https://doi.org/10.1007/BF02394719, 1990.

Stanford, J. A., Lorang, M. S., and Hauer, F. R.: The shifting habitat mosaic of river ecosystems. Internationale Vereinigung für theoretische und angewandte Limnologie: Verhandlungen, Int. Ver. The., 29, 123–136, https://doi.org/10.1080/03680770.2005.11901979, 2005.

Steger, C., Kotlarski, S., Jonas, T., and Schär, C.: Alpine snow cover in a changing climate: a regional climate model perspective, Clim. Dynam., 41, 735–754, https://doi.org/10.1007/s00382-012-1545-3, 2013.

Stewart, I. T.: Changes in snowpack and snowmelt runoff for key mountain regions, Hydrol. Process., 23, 78–94, https://doi.org/10.1002/hyp.7128, 2009.

Stewart, I. T., Cayan, D. R., and Dettinger, M. D.: Changes in snowmelt runoff timing in western North America under a "Business as Usual" climate change scenario, Climatic Change, 62, 217–232, https://doi.org/10.1023/B:CLIM.0000013702.22656.e8, 2004.

Stewart, I. T., Cayan, D. R., and Dettinger, M. D.: Changes toward earlier streamflow timing across western North America, J. Climate, 18, 1136–1155, https://doi.org/10.1175/JCLI3321.1, 2005.

Takaoka, S. and Swanson, F. J.: Change in extent of meadows and shrub fields in the central western Cascade Range, Oregon, Prof. Geogr., 60, 527–540, https://doi.org/10.1080/00330120802212099, 2008.

Tape, K. E., Sturm, M., and Racine, C.: The evidence for shrub expansion in Northern Alaska and the Pan-Arctic, Glob. Change Biol., 12, 686–702, https://doi.org/10.1111/j.1365-2486.2006.01128.x, 2006.

Tennesen, M.: When juniper and woody plants invade, water may retreat, Science, 322, 1630–1631, https://doi.org/10.1126/science.322.5908.1630, 2008.

Theurillat, J. P. and Guisan, A.: Potential impact of climate change on vegetation in the European Alps: a review, Climatic Change, 50, 77–109, https://doi.org/10.1023/A:1010632015572, 2001.

Valeo, C., Xiang, Z., Bouchart, F. C., Yeung, P., and Ryan, M. C., Climate change impacts in the Elbow River watershed, Can. Water Resour. J., 32, 285–302, https://doi.org/10.4296/cwrj3204285, 2007.

Vincent, L. A., Zhang, X., Brown, R. D., Feng, Y., Mekis, E., Milewska, E. J., Wan, H., and Wang, X. L.: Observed trends in Canada's climate and influence of low-frequency variability modes, J. Climate, 28, 4545–4560, https://doi.org/10.1175/JCLI-D-14-00697.1, 2015.

Vogl, R. J.: One hundred and thirty years of plant succession in a southeastern Wisconsin lowland, Ecology, 50, 248–255, https://doi.org/10.2307/1934852, 1969.

Wang, G., Cai, W., Gan, B., Wu, L., Santoso, A., Lin, X., Chen, Z., and McPhaden, M. J.: Continued increase of extreme El Niño frequency long after 1.5 C warming stabilization, Nat. Clim. Change, 7, 568–572, https://doi.org/10.1038/nclimate3351, 2017.

Wang, X., Helgason, B., Westbrook, C., and Bedard-Haughn, A.: Effect of mineral sediments on carbon mineralization, organic matter composition and microbial community dynamics in a mountain peatland, Soil Biol. Biochem., 103, 16–27, https://doi.org/10.1016/j.soilbio.2016.07.025, 2016.

Wang, X., Shaw, E. L., Westbrook, C. J., and Bedard-Haughn, A.: Beaver dams induce hyporheic and biogeochemical changes in riparian areas in a mountain peatland, Wetlands, 38, 1017–1032, https://doi.org/10.1007/s13157-018-1059-9, 2018.

White, J. C., Wulder, M. A., Hobart, G. W., Luther, J. E., Hermosilla, T., Griffiths, P., Coops, N. C., Hall, R. J., Hostert, P., Dyk, A., and Guindon, L.: Pixel-based image compositing for large-area dense time series applications and science, Can. J. Remote Sens., 40, 192–212, https://doi.org/10.1080/07038992.2014.945827, 2014.

Whitfield, P. H.: Linked hydrologic and climate variations in British Columbia and Yukon, Environ. Monit. Assess., 67, 217–238, https://doi.org/10.1023/A:1006438723879, 2001.

Whitfield, P. H.: Climate station analysis and fitness for purpose assessment of 3053600 Kananaskis, Alberta, Atmos. Ocean, 52, 363–383, https://doi.org/10.1080/07055900.2014.946388, 2014.

Windell, J. T. and Segelquist, C.: An ecological characterization of Rocky Mountain montane and subalpine wetlands, 86, Fish and Wildlife Service, US Department of the Interior, https://apps.dtic.mil/sti/tr/pdf/ADA323499.pdf (last access: 30 November 2022), 1986.

Wulder, M. A., Roy, D. P., Radeloff, V. C., Loveland, T. R., Anderson, M. C., Johnson, D. M., Healey, S., Zhu, Z., Scambos, T. A., Pahlevan, N., Hansen, M., Gorelick, N., Crawford, C. J., Masek, J. G., Hermosilla, T., White, J. C., Belward, A. S., Schaaf, C., Woodcock, C. E., Huntington, J. L., Lymburner, L., Hostert, P., Gao, F., Lyapustin, A., Pekel, J.-F., Strobl, P., and Cook, B. D.: Fifty years of Landsat science and impacts, Remote Sens. Environ., 280, 113195, https://doi.org/10.1016/j.rse.2022.113195, 2022.

Yang, Y., Gan, T. Y., and Tan, X.: Recent changing characteristics of dry and wet spells in Canada, Climatic Change, 165, 42, https://doi.org/10.1007/s10584-021-03046-8, 2021.

Zhang, T., Li, D., East, A. E., Walling, D. E., Lane, S., Overeem, I., Beylich, A. A., Koppes, M., and Lu, X.: Warming-driven erosion and sediment transport in cold regions, Nat. Rev. Earth Environ., 3, 1–20, https://doi.org/10.1038/s43017-022-00362-0, 2022.

Zhang, X., Vincent, L. A., Hogg, W. D., and Niitsoo, A.: Temperature and precipitation trends in Canada during the 20th century, Atmos. Ocean, 38, 395–429, https://doi.org/10.1080/07055900.2000.9649654, 2000.

Zhou, Z. Q., Xie, S. P., Zheng, X. T., Liu, Q., and Wang, H.: Global warming–induced changes in El Niño teleconnections over the North Pacific and North America, J. Climate, 27, 9050–9064, https://doi.org/10.1175/JCLI-D-14-00254.1, 2014.